Design of a new yttrium silicate Environmental Barrier Coating (EBC) based on the relationship between microstructure, transport properties and protection efficiency

Simon Arnal, Sébastien Fourcade, Fabrice Mauvy, Francis Rebillat

Design of a new yttrium silicate Environmental Barrier Coating (EBC) based on the relationship between microstructure, transport properties and protection efficiency

S. Arnal[a], S. Fourcade[b], F. Mauvy[b], F. Rebillat[a]

a Laboratoire des Composites ThermoStructuraux (LCTS), Université de Bordeaux, UMR 5801, 3 allée de la Boétie, 33600 Pessac, France

b Institut de Chimie de la Matière Condensée de Bordeaux (ICMCB), CNRS, Université de Bordeaux, UMR 5026, 87 Avenue du Dr Albert Schweitzer, 33600 Pessac, France

Keywords : environmental barrier, silicate, conductivity, recession, microstructure, diffusion coefficient

ABSTRACT

Yttrium mono- and di-silicates are excellent candidate materials for Environmental Barrier Coatings (EBC), to protect Ceramic-Matrix Composites (CMC). A large distribution of microstructures can be generated by varying the duration of sintering, the particle size distribution of the precursor and/or the deposition method. In the present work, investigations of the corrosion resistance of yttrium silicate coatings with various microstructures in the high temperature range, under different oxidizing environments are reported. An original experimental methodology has allowed quantifying the influence of the microstructure (especially grain size and grain boundary surface area) on properties such as ionic conductivity, resistance to oxygen diffusion, volatilization rate and surface recession, and showing that they directly affect their protection efficiency against oxidation. Based on these results, guidelines for the design of an optimized yttrium silicate EBC featuring microstructural and compositional variations are proposed.

1 - Introduction

Over the past four decades, the oxidation of steel in super-heaters has dramatically affected the integrity of many high-temperature devices. Almost all coal fired plants, boilers and gas turbines have been affected by hot corrosion with dry or wet oxygen or air, reducing drastically the equipment lifetime. Future generations of turbine elements currently composed of super alloys are considered to be replaced by Ceramic Matrix Composites (CMCs) [1,2]. Generally, these CMCs consist of a SiC-based ceramic matrix reinforced with carbon or silicon carbide fibers. CMCs are chosen because of their high thermal and mechanical properties. At elevated temperatures and under severe environments, silicon carbide present in the matrix reacts with di-oxygen (O_2) and water vapor (H_2O) in the atmosphere to form a passivation silica scale [3]. However, in presence of moisture at elevated temperature under high gas velocity, volatilization of silica occurs and may cause an excessive surface recession leading to a higher silicon carbide consumption rate and to the lowering of mechanical properties of the composite [4]. It then follows a strong degradation of the material element. To protect CMCs from these phenomena induced by severe environments, Environmental Barrier Coatings (EBCs) are used. The most stable EBCs are often Rare-Earth (RE) silicates [5,6] usually yttrium disilicate (YDS) and monosilicate (YMS); they have extremely low oxygen permeation rates, have low thermal conductivity, have suitable mechanical properties and their Coefficients of Thermal Expansion (CTE) match the ones of CMCs [7-11].

As mentioned in previous studies, combining experimental data and a thermodynamic approach, YDS and YMS have a stability in humid air almost 7 times greater than silica [12-14]. Yttrium silicates also reportedly present a good resistance to the surface volatilization or to corrosion by Calcium-Magnesium-Aluminum-Silicate sands (CMAS) [6,14-29].

In the binary diagrams between rare earth oxides and silica, there are three defined compounds: the rare earth monosilicate RE_2SiO_5, the disilicate $RE_2Si_2O_7$ and the oxyapatite $RE_4Si_3O_{12}$ [26]. Each of these defined compounds has different characteristics (crystallography, melting temperature, etc.) which directly influence their properties for applications as EBCs [2-33]. Monosilicates are composed of two types of anions $(SiO_4)^{4-}$ and O^{2-} and a rare earth cation RE^{3+} to form an arrangement of tetrahedra of (SiO_4) and $(O\text{-}RE_4)$. The disilicates are themselves composed of double tetrahedra $(SiO_7)^{6-}$ and rare earth cations RE^{3+} and have several polymorphs [27].

EBCs are usually deposited on the CMC surface over a bond coat layer, most frequently made of silicon; after having been exposed some time to an oxidizing environment, a Thermally Grown Oxide (TGO) layer develops at the interface between the Si bond coat and the RE silicate layer. In favorable situations, TGO growth is limited by oxygen transfer through the EBC, which occurs by diffusion. O_2 and H_2O molecular forms may diffuse within the cracks but also in dense materials in ionic forms according to the migration of O^{2-} and OH^- anions in the crystalline network of the material. It is desirable to limit the O^{2-} and OH^- diffusivity of the coating because the growth of TGO under the coating leads to spallation of the layer and slowing the diffusion of ions reduces the rate of growth of TGO. As a consequence, the characterization of the mobility through the material of ionic species by the ionic conductivity is very important [34-37].

In addition, to better understand the surface exchange of oxygen over an oxide material and its transport into the material (volume diffusion), $^{18}O_2$ tracer diffusion experiments have been performed and Secondary Ion Mass Spectrometry (SIMS) has been used to determine oxygen diffusivities [38-40]. Many authors working on ionic and mixed ionic-electronic conductors for Solid Oxide Fuel Cells (SOFC) [41-43] carried out isotopic exchanges in order to evaluate the effective oxygen coefficient (D_O) in their materials. This technique has mostly been used with relatively well-conducting oxides; very few authors have been interested in the diffusion coefficient of oxygen in insulating ceramics [38, 44, 45]. The ef-

fective oxygen diffusion coefficient can reach extremely low values $D_O = 6.10^{-18}$ $m^2.s^{-1}$ at 1300 °C in yttrium monosilicate single crystals, which confirms their good potential as EBCs. Furthermore, among silicates, a decrease of the recession rate can be obtained by the selection of a rare earth with smaller ionic radius [38, 44, 45]. For instance, lutetium disilicate (ionic radius of Lu = 86 pm) is less sensitive to volatilization phenomena than yttrium disilicate (ionic radius of Y = 90 pm). According to literature data [46-49], the formation of a monosilicate layer above a disilicate coating allows contributing to limit surface recession, by changing the chemical composition and the microstructure of the surface [50]. Indeed, monosilicates have a lower recession rate than disilicates. However, RE silicate-based EBCs are polycrystalline, contain defects, pores and display microstructural inhomogeneity, which can deeply influence the effective diffusion coefficient and consequently on the recession rates.

In the literature, the influence of the microstructure on transport properties in ceramics [30] has been demonstrated, in particular in Yttria Stabilized Zirconia (YSZ). In thin films, a nanostructured and equiaxial microstructure developed by Spark Plasma Sintering (SPS) has been shown to be more resistive than a columnar microstructure with a preferential direction [30]. In the columnar microstructure, the absence of tight grain boundaries between the columns forms preferential diffusion pathways. On the other hand, in the nanostructured and equiaxial microstructure, the migrating species are forced to cross grain boundaries, which can be considered to act as barrier layers. Inside conductive oxides like YSZ, a grain boundary is a diffusion barrier that greatly limits the ionic conductivity [31]. By decreasing the grain size, the surface of grain boundaries is increased and the ionic conductivity of the material is lowered [32, 33, 41]. The grain boundary appears as a place where the concentration of oxygen vacancies decreases sharply. The grain boundaries are sinks of oxygen vacancies and thus generate depletion areas of oxygen vacancies around them. By dramatically decreasing the concentration of oxygen vacancies near the grain boundary, there is a large decrease in the number of possible "jumps" for migrating atoms [32]. Moreover, the energy required to perform the step-by-step jump is increased, which

results in an increase in the activation energy. In rare earth apatites, known for their high ionic conductivity (they are promising materials for SOFC), a similar influence on conductivity is reported on dense samples processed by sintering: with micrometric grains, the conductivity is 10 times higher than with a nanometer-sized microstructure [42-43].

To sum up, very few studies report quantitative data on the protection efficiency of RE mono- and disilicate based EBC coatings against oxidation and water vapor corrosion, especially in relation with their microstructure. Actual data on oxygen diffusion through EBC materials, which display a complex microstructure, are not available in many cases. To characterize ionic conductivity in the ceramic coatings, Electrochemical Impedance Spectroscopy (EIS) is a classical method. Because it is easy to set up, cheap, non-destructive and very sensitive to the materials transport properties, this technique is widely used in solid state electrochemistry. Indeed, it makes it possible to determine the transport properties of the material such as ionic conductivity (separating bulk and grain boundaries contributions) and/or the electrode reaction kinetics such as gas electrode properties as a function of temperature, oxygen pressure, and microstructure [40,51-55].

The aim of the present work is to better understand the relations between the transport properties (ionic conductivity and/or effective diffusion coefficient) and the recession rate of yttrium silicates with varying microstructures and compositions. For this, ceramic samples with different microstructures have been prepared and a new methodology is introduced. The idea is to obtain by two distinct methods estimates of the diffusion coefficient of species through the EBC.

We propose to characterize the ionic conductivity by Electrochemical Impedance Spectroscopy measurements, which has not yet been attempted on this type of materials so far. This technique will be used to study chemical stability and ageing processes by measuring the evolution of the impedance at a given

temperature according to the time duration. The goal is then to compare ionic conductivity measurements by EIS on massive oxide materials and effective diffusion properties under corrosion atmosphere. Recession rates have been determined from mass loss during corrosion tests. Further, model samples based on layered composite structure (EBC/Si/EBC) have been designed. By following the oxidation of silicon (TGO growth), the efficiency of the EBC to protect a CMC by limiting the diffusion of oxidizing species has been quantified.

2 - Materials and methods

2.1 Samples design

Single phase model samples have been prepared in this work to give access to the specific properties of materials and to compare between yttrium monosilicate (YMS) and disilicate (YDS), with different microstructures. Two types of specimen geometries were chosen to study respectively: the recession rate and the protection efficiency of silicates under high temperatures conditions. For recession tests and ionic conductivity measurements, the materials samples were in the form of pellets with a diameter between 10 mm and 15 mm and a thickness between 1 mm and 2 mm. For the estimation of protection efficiency, model coatings were part of a "sandwich"-type structure made of a Si pellet embedded in silicate, i.e. a $Y_2Si_2O_7$/Si/$Y_2Si_2O_7$ tri-layer, where the substrate of silicon is protected on each face by a layer of EBC material (detailed in part 2.3 and Figure 1). The choice of Si for the pellet was motivated by the fact that Si is used as bond coat on a CMC; additionally, it allows the measurement of diffusion through the EBC thanks to the measurement of TGO growth kinetics.

Ceramic samples pellets were made of YMS, YDS and YDS-30%vol. Yttrium Oxy-Apatite (YOA) materials.

Monolithic Yttrium silicate samples were also prepared for high-temperature corrosion tests in order to characterize the surface morphologies after the tests.

Samples of well-known materials also have been synthesized for sake of comparing conductivities: (1) Yttria Stabilized Zirconia (8YSZ, ZrO_2-8%Y_2O_3, here with a relative density close to 95%), widely used as a thermal barrier (TBC) on the blades of metal turbines and (2) Barium Strontium Alumino-Silicate (BSAS, (1-*x*)BaO • *x*SrO •Al_2O_3 •2SiO_2), a material for the second generation of EBCs.

2.2 Powder synthesis

To get yttrium silicates (monosilicate and disilicate) under a thin powder form, a sol/gel route was chosen. This method has been selected in the aim of obtaining a pure compound with the expected polymorph. The sol-gel method consists in synthesizing a solid powder by means of solution precursors [46-47]. The principle is based on the succession of hydrolysis-condensation reactions to form networks of oxides which are then heat-treated. Several precursors exist to form rare earth silicates: the reaction is possible starting with alkoxide precursors dissolved in isopropanol [48] or precursors in the form of nitrates dissolved in a tetraethylorthosilicate (TEOS) [49].

In the present work, the sol-gel process used was essentially the same as the one described by Chrysafi [50]. Colloidal silica was selected as silica source instead of TEOS. A RE nitrate $RE(NO_3)_3$ • xH_2O was dissolved in a minimum amount of water with stirring. The silica was then added in stoichiometric proportion to obtain either the monosilicate or the disilicate of the rare earth considered (ratio 1:1 for the monosilicate and 1:2 for the disilicate). The whole was then heated with stirring at 70°C for 4 h, to get the gel form. After drying and calcination at 900°C for 5 hours allowing the last organic ligands to be released, an amorphous powder made up of aggregates was obtained. To obtain the desired polymorph

for yttrium disilicate (γ phase) and yttrium monosilicate (X2 phase), heating treatments were performed in air at temperatures higher than 1400°C during up to 50 h (detailed in part 2.4 and Figure 2).

As expected, during the heating treatment, the grains have undergone granular coalescence and numerous sintering necks have formed. Thus, grinding (E_{MAX} from Retsch) was essential to obtain a powder of submicron size with a higher specific surface and reactivity during sintering. It is a high energy mill using grinding speeds of up to 1500 rpm. In this device, zirconia bowls and grinding balls (diameter of the balls = 500 μm) were used. The solvent was water. The grinding time was 1 h, alternating grinding sequences of 5 min at 1500 rpm and 5 min at 300 rpm to avoid excessive heating of the bowls, the grinding balls and the solvent. The particles size distribution (PSD) of the powder after grinding was submicronic, monomodal and centered around an average grain size of 0.7 μm.

2.3 Elaboration of tested samples

The specimens were processed by Spark Plasma Sintering (SPS, Dr. Sinter Lab model 511/515) and by classical natural sintering in air. The SPS sintering conditions for the pellets were as follows. A first heating was carried out up to 600°C in a "blind" mode (600°C is the pyrometer lower detection limit) and continued up to 1000°C at 80°C.min^{-1}. The second ramp was 50°C.min^{-1} up to the target temperature, i.e. 1400°C, followed by a 5-min dwell period. Cooling down was made at the rate dictated by the furnace thermal inertia. The pressure applied during the whole cycle was 100 MPa.

For the "sandwich"-type geometries, a Si pellet (poly-crystallized wafer) is embedded in a powder bed of silicate. Then, the SPS cycle was identical except that the maximum sintering temperature was limited to 1250°C due to the presence of silicon, which has a melting point at 1415°C.

In the "sandwich"-type samples, the final thickness of each disilicate layer after sintering was approximately 500 μm. A summary of these elaboration process and a view of this sample geometry are

available on Figure 1. When a classical natural sintering in air is used, a larger grain size is obtained and a thin TGO scale is formed at surface of the silicon pellet.

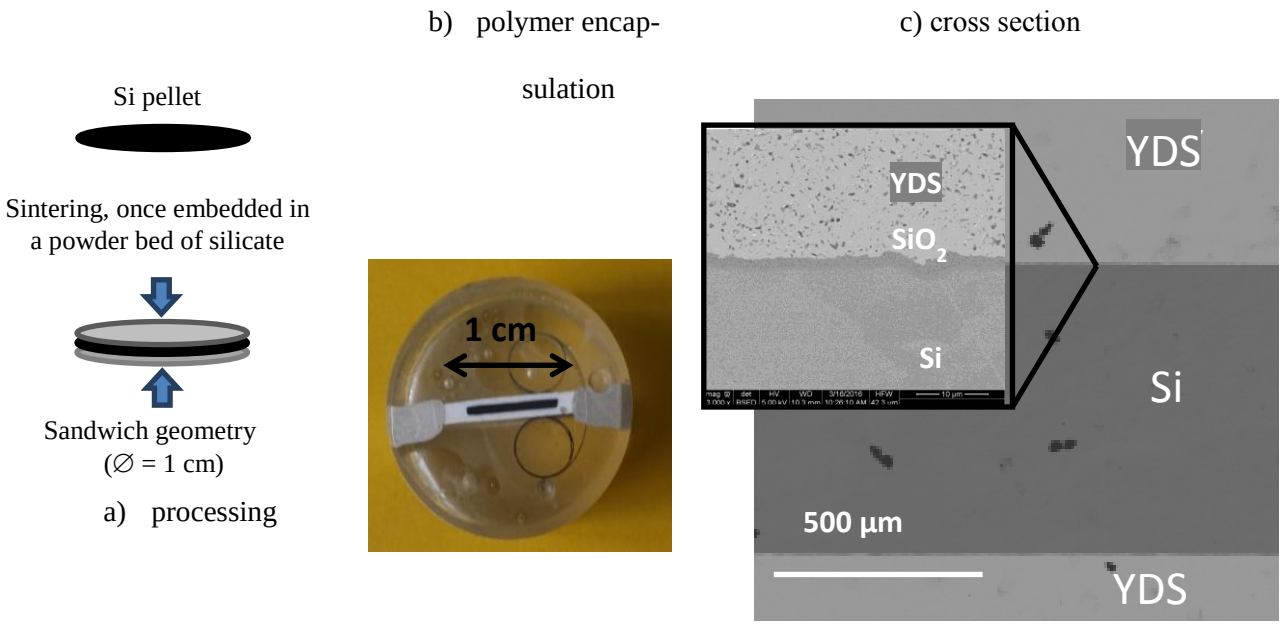

Figure 1: Fabrication process of the "sandwich"-type sample geometry: a) processing, b) polished cross section in a resin encapsulation (yttrium disilicate in white fully covering silicon in black) and c) micrograph of Si/YDS interfaces, with the presence of a silica layer when a classical natural sintering in air is performed

2.4 Structural, chemical and morphological characterizations

The X-ray diffraction technique makes possible to obtain information on the structures, the phases, the preferred orientation of the crystallites, the average size of the crystallites and the state of crystallization of the materials. A Bruker D8 Advance diffractometer, with a copper anticathode, has been used. The measurement mode was Bragg-Brentano or parallel beam. The search for phases corresponding to the

diffraction peaks had been carried out automatically using the EVA software and the JCPDS-ICDD database.

In this work, XRD was used to control the purity (mostly, absence of potential pollution by ZrO_2 from the grinding step) and the crystallinity of the powder throughout the production stages and to check that only the desired polymorph (γ for YDS ; JCPDS-ICDD 04-015-5861 and X_2 for YMS : JCPDS-ICDD 00-038-023) is present in each material.

The coatings were also imaged using a Scanning Electron Microscope (SEM) (FEI 400 FEG). The Electron Back-Scattering (EBS) analysis mode was mainly used to qualify the homogeneity of different elements (by deduction: constituents) across the samples and the potential presence of impurities. The grain size was evaluated from SEM snapshots using Image J software. An Electron Dispersion Spectroscopy (EDS) probe was used to carry out point measurements or maps to check the chemical composition and its homogeneity.

In this work, the AFM will allow to observe where the corrosion phenomena (consumption of EBC) are located in order to identify the zones the least resistant to degradation process, in connection with the microstructure. Characterizations were performed on monolithic silicate materials with different grain sizes Initially, one surface was polished to get low roughness (Ra of around few nanometers). After ageing, AFM characterizations were done to locate where the volatilization over the material surface took place.

The porosity ratio was measured by helium pycnometry (Micromeritics AccuPyC 1330).

2.5 Electrochemical Impedance Spectroscopy (EIS) measurements

This method. widely used in solid state electrochemistry. Indeed, it makes possible to determine the transport properties of the material such as ionic conductivity (bulk and grain boundaries contributions)

and/or the electrode reaction kinetic such as gas electrode properties as a function of temperature, oxygen pressure, and microstructure.

EIS measurements were carried out on the dense ceramic pellets. Before a measurement, two symmetrical platinum electrodes are painted and sintered on both sides of a pellet. Then, the pellet is placed inside a dedicated furnace with controlled temperature and atmosphere between two platinum grids used as current collectors. A sinusoidal voltage U is applied to the sample, which is then fully traversed by an alternating electric field, and the resulting alternating current I is measured. From the ratio between voltage and current, the impedance of the system is extracted using Ohm's law in alternative mode:

$$Z(\omega) = \Delta U(\omega) / \Delta I(\omega) \qquad (1)$$

Measurements were carried out across the widest allowed frequency range (10^6 Hz > f > 0.1 Hz) to observe the largest possible number of phenomena. According to the Nyquist representation, the results are plotted in a complex plan (Z ', - Z"), as reported on Figure 2. In order to identify the experimental data, the impedance diagram is then modeled using an electrical equivalent circuit consisting of associated elements (resistances (R), inductances (L), capacitances (C), constant phase elements (CPE), …). After data fitting, the real part of the impedance has been used to determine the conductivity of the sample thanks to the following relation (2):

$$\sigma = \frac{1}{R} \times \frac{\delta}{S} \qquad (2)$$

With:

σ = conductivity ($S.m^{-1}$)

δ = thickness of the material or deposit (m)

R = identified resistance (Ω)

S = electrode surface area (m^2)

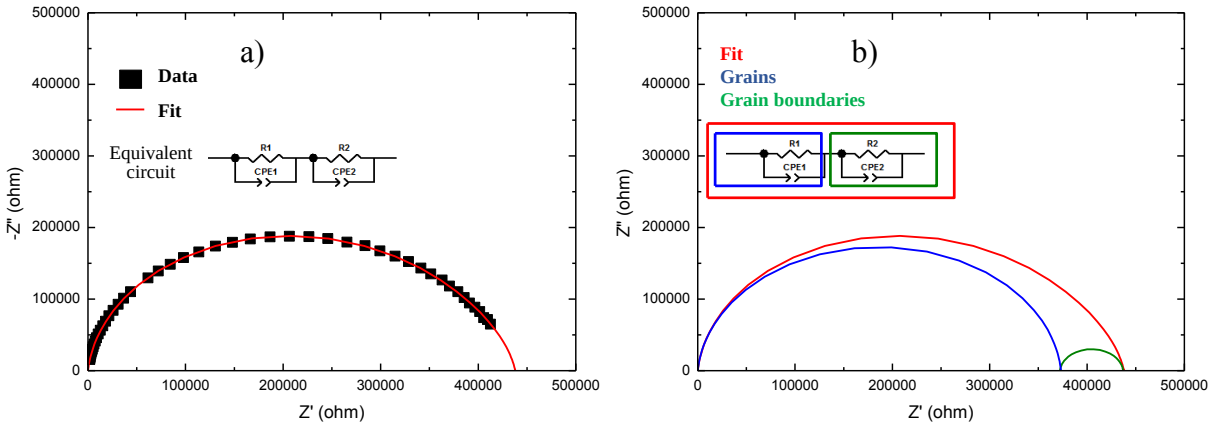

Figure 2: Typical impedance diagram of yttrium disilicate ceramic sample (~ 9µm grain size), measured by EIS, at 777°C in dry air: a) Nyquist representation: raw data (filled squares) and global fit using an equivalent circuit and b) deconvolution into 2 main contributions: bulk and grain boundaries.

This technique is also used to study chemical stability and ageing processes by measuring the evolution of the impedance at a given temperature according to the time duration.

2.6 Oxidation/corrosion tests and characterization

High temperature oxidation tests were first carried out under dry air at 1300°C: in a simple configuration dioxygen is the only oxidizing species. Later, corrosion tests were performed at 1300°C and 1400°C in moist air under a total pressure of 100 kPa with a water vapor partial pressure of 50 kPa (10 kPa O_2 and 40 kPa N_2), during testing times up to 600 hours. In order to supply air with steam, dry air goes through a pre-saturating system at room temperature (P_{H_2O} ~ 2-3 kPa), then through a heating column maintained at 81°C to obtain the desired water vapor partial pressure (P_{H_2O} = 50 ± 1 kPa). This particular temperature was chosen using a water vapor saturation pressure table. The water vapor partial pressure in the corrosive atmosphere was verified by measuring the quantity of liquid water carried

away by the dry air flow during the test. The oxygen partial pressure represents 20% of the complementary pressure to attain the atmospheric pressure (P_{O_2} = 0.2 × (P_{atmc}- P_{H_2O}) = 10 kPa). The value of gas flow velocity is 5 cm.s^{-1} in the cold zone of the furnace or around 28 ± 1 cm.s^{-1} in the hot zone. Samples are introduced in the alumina tube (inner diameter: 34 mm, purity: 99.7 %, OMG, France) of the furnace, on YSZ plates to avoid possible reactions with alumina.

To determine the volatilization rate from such corrosion tests, the surfaces of pellets were polished to mirror state (R_a of around few nanometers) in order to get well-defined and reproducible reactive surface areas. The experiment durations are limited to a few hours, to avoid a significant pollution (as aluminates) of the surface by reaction with $Al(OH)_3$, formed itself by reaction of the Al_2O_3 furnace tube with moisture, as previously observed in the literature [56, 57].

Evaluation of protection efficiency

The "sandwich"-type geometries samples with model coatings were developed to access to experimental values of diffusion coefficient. The goal was to compare to ionic conductivity measurements by complex impedance spectroscopy on massive oxide materials and effective diffusion properties under corrosion atmosphere. To quantify the protection efficiency of silicates as EBCs, the oxidation rate of Si pellets in sandwich geometries (i.e. under a silicate layer) has been determined.

The comparison between the oxidation behaviors of a coated silicon with yttrium di-silicate and an as-received silicon pellet allowed highlighting the efficiency of protection of the EBC material in reducing the gas diffusion up to the Si pellet. After selected temperature and ageing duration, samples are cut in two parts and the thickness of silica layer formed at the interface DSY/Si was measured using SEM im-

ages (Figure 1). The growing rate of the silica layer formed by oxidation of Si is used to evaluate the protection efficiency of the EBC material.

The global recession rate is deduced from weight losses during ageing tests.

In a previous study performed with this equipment with a similar gas flow rate, it had been checked that the evacuation of produced hydroxides over the sample occurred by convection, through the geometric surface [12-14]. Knowing the sample surface area in contact with the moist environment, the oxide volatilization rate was derived directly from the weight loss/surface ratio as a function of working time. On such a short time of corrosion, the volatilization disilicate can be considered as complete without the formation of a residual monosilicate layer (not significant, since not observed) [12,13].

3 – Results

3.1 Structure, morphology and composition of the samples

In this work, DRX was used to control the purity and the crystallinity of the powder throughout the production stages (Figure 3). The DRX will ensure that only the desired polymorph (γ for DSY and X2 for MSY) is present in each material. After each processing step, no pollution was detected by XRD, as ZrO_2 from grinding.

As expected, the fired xerogel was amorphous. γ-$Y_2Si_2O_7$ was the only polymorphic form after a heating treatment at least at 1400°C for 50 hours in air.

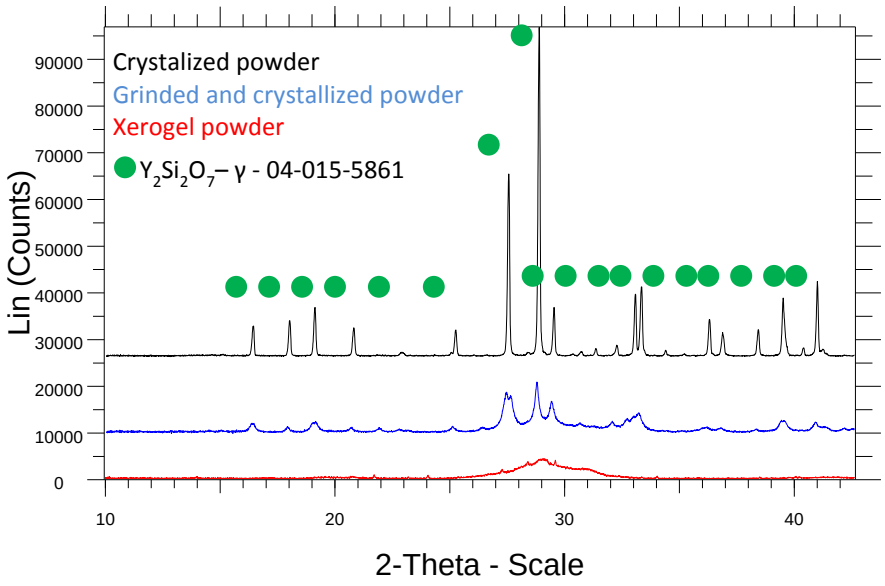

Figure 3: X-ray diffraction pattern of the sol/gel powder of yttrium disilicate at different steps during the elaboration: xerogel, crystallised powder and grinded crystallised powder

Further, different microstructures of disilicate have been obtained by variation of the sintering conditions (times and temperatures) (Table 1). The effect of temperature and time on the coalescence phenomena can be observed on Figure 4. The grain sizes overcome 10 µm after the heating treatment at the highest temperature and the longest time (Table 1).

Table 1: Sintering conditions, grain size and relative porosity of yttrium disilicate (to get various microstructures – see Figure 3).

Material	1	2	3	4
Sintering method	SPS	Conventional	Conventional	conventional
Heating treatment	1400°C 5 min under vacu-	1400°C 50 h in air	1500°C 50 h in air	1500°C 150 h in air

	um			
Grain size (µm) Standard deviation	0.8 ±0.1	2.7 ±1.1	4.2 ±1.5	10.9 ±4.4
Relative porosity (%)	8	6	6	4

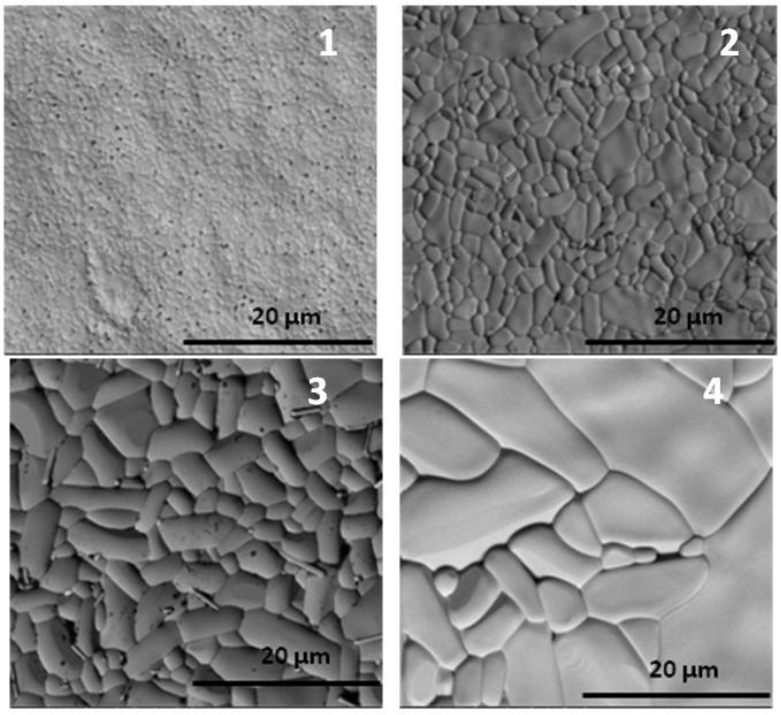

Figure 4: SEM images and microstructures observed with the different pellets of disilicate, sintered at different times and temperatures (see Table 1)

3.2 Ionic transport properties

Comparison of oxygen ionic conductivities into EBC/TBC materials

The values of ionic conductivity were deduced from EIS measurements performed at various temperatures in dry air, on YDS, 8YSZ (ZrO_2-8%Y_2O_3 - YSZ with relative density close to 95%) and BSAS ((1-x)BaO.xSrO.Al_2O_3.2SiO_2) ceramic samples with a similar grain size, close to Φ_{grain} ~ 5 µm. The results are reported on Figure 5 as an Arrhenius plot. Using the present set-up, accurate measurements could not be obtained for ionic conductivities below $\sigma < 2.10^{-7}$ S.cm^{-1}. As a consequence, only few points are available for very resistive materials. Figure 5 shows that yttrium disilicate has a much lower ionic conductivity than 8YSZ by about five orders of magnitude ($\sigma_{YDS} = 2.10^{-7}$ S.cm^{-1} $\sigma_{YSZ} = 1.10^{-2}$ S.cm^{-1} at 1000°C). Concerning 8YSZ, the obtained results agree with literature data [36, 58]. Indeed, the substitution of zirconium by yttrium leads to the creation of oxygen vacancies contributing to considerably increase the ionic conductivity. On the other hand, the values of ionic conductivity of YDS are very low and are smaller than those of BSAS, confirming YDS as a potentially efficient material to limit the diffusion of oxidizing species. Reversely, YSZ appears as an excellent oxygen ion conductor especially in the high temperature range. These first results confirm the choice of YDS in regard to references materials in this field: 8YSZ and BSAS.

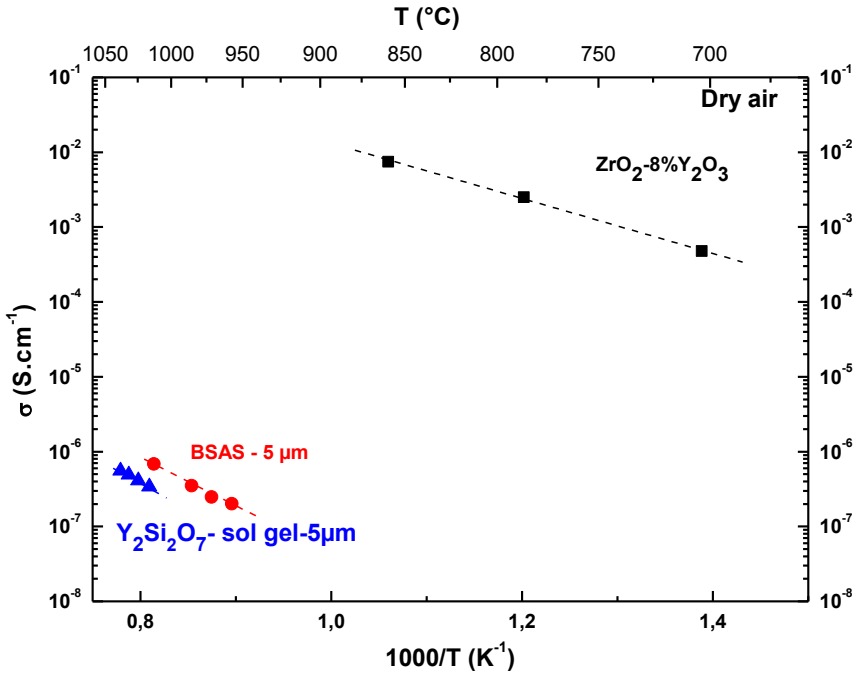

Figure 5: Arrhenius plots of ionic conductivity measured by EIS of yttrium disilicate, BSAS an Yttria Stabilized Zirconia (8YSZ), at high temperature in dry air (N_2/O_2=80/20) and a ~5µm grain size.

Influence of the grain size on the ionic conductivity of yttrium disilicate

The same type of oxygen ionic conductivity measurements has been performed on YDS pellets with different grain sizes, and considering similar relative porosity (around 6%). The goal was to better understand the relationship between the oxygen transport properties and the ceramic microstructure. The grain size has been controlled through the temperature and the duration of the sintering, as described previously. According to the Arrhenius curves reported on Figure 6, the modification of grain size (in the range 2µm $< \Phi_{grain} <$ 9µm) appears as a significant factor influencing O^{2-} conductivity. The data have been fitted (χ^2 = 0.0015) with the following expression (equation (3)):

$$\sigma = 8.97 \exp(-[23360 - 1500\ \Phi_{grain}]/T)\ \Phi_{grain}^{0.34} \qquad (3)$$

where σ is in $S.cm^{-1}$ and Φ_{grain} being the grain diameter in µm. The activation energy is (2.014 – $0.129\Phi_{grain}$) eV. The comparison of ionic conductivity values for each material shows that a reduction in grain size leads to a significant decrease in oxygen conductivity. The sample with a grain size of Φ_{grain} ~ 1 µm has an ionic conductivity about 10 times lower than the pellet with a grain size close to Φ_{grain} ~ 9 µm. Respectively, the value of activation energy increases when the grain size decreases. The conductivity mechanism thus seems to require more energy to take place. As the associated surface area of grains boundaries increases with the decrease of the grain size, the density of grain boundaries could be responsible for this behavior. These results show that grain boundaries may act as diffusion barriers towards ionic species. These observations agree with many previous works on various oxides [32, 33,41-45].

a)

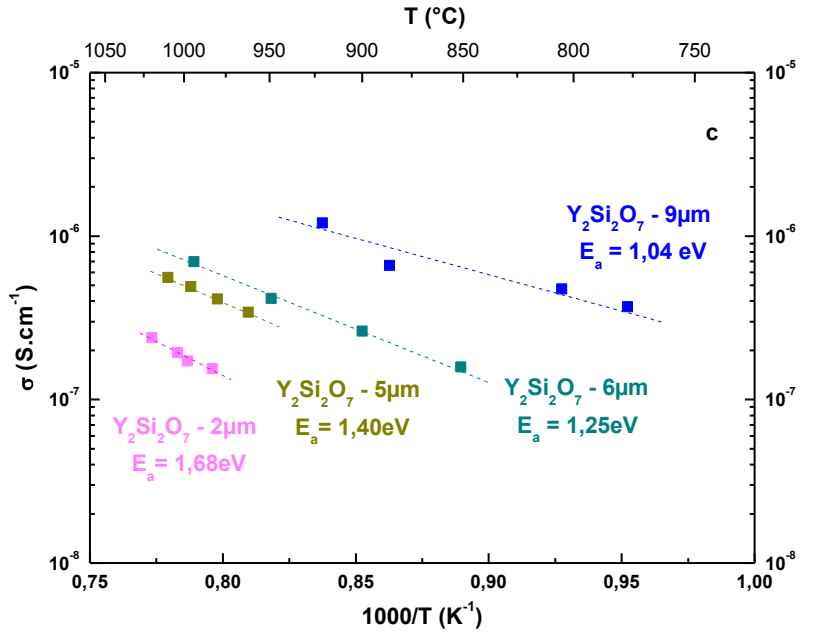

b)

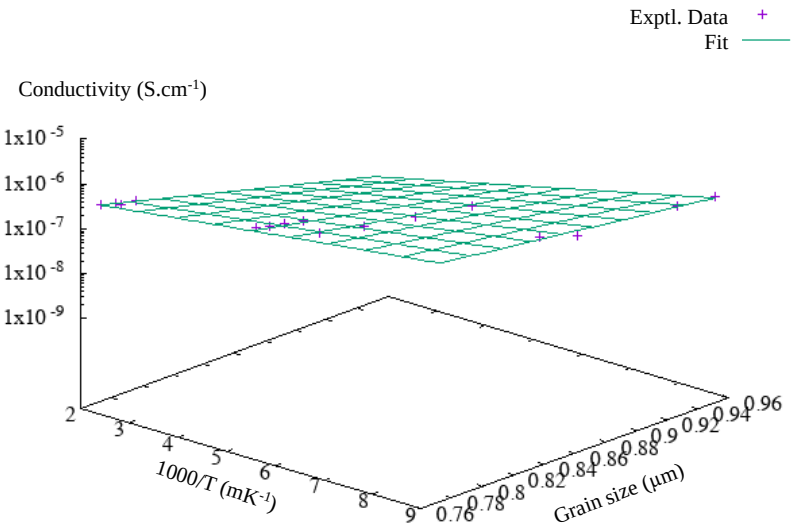

Figure 6: Ionic conductivity measured by EIS of yttrium disilicate with different grain sizes (obtained by a sol-gel route and sintered), at high temperature in dry air (N_2/O_2=80/20): a) Arrhenius plots and b) 3D-fit of the conductivity *vs.* grain size and temperature

Ionic conductivity of different silicate materials

Among the factors influencing ionic conductivity of EBCs, the structural types of single-phase yttrium silicates YMS, YDS, or yttrium oxy-apatite (YOA), and their mixtures have also to be considered. Thus, conductivity measurements were carried out on monolithic materials with iso-microstructure (grain size around Φ_{grain} ~ 5µm and relative porosity close to 6%) (see Figure 7). As previously described, ceramic samples pellets were made of YMS, YDS and YDS-30%vol.YOA materials and densified by conventional sintering. The associated ionic conductivity properties are plotted against temperature in Figure 8. Considering similar microstructures, the disilicate phase possesses the lowest ionic conductivity. Monosilicate appears as a slightly better ionic conductor than disilicate. This observation can be explained by the difference in crystallographic structure and the type of bonds present in the material, in particular between silicon and oxygen groups [16-19, 26-33]. In the disilicate, the silicon groups involved are Si_2O_7 whereas in the monosilicate these groups are present in the SiO_4 form. The creation of oxygen vacancies would be easier in monosilicate (less stable) than in disilicate. This slight increase in the point defect concentration would explain the increase in the ionic conductivity of monosilicate relative to disilicate. As a consequence, disilicate material can be considered as the most effective barrier to the diffusion of oxidizing species.

According to Figure 7, it can also be noticed that the presence of yttrium oxy-apatite as a secondary phase in the sample material leads to a considerable increase in the ionic conductivity of this material. The high conductivity of apatite is mainly due to its hexagonal crystalline structure, which presents conduction pathways that are favorable to the mobility of O^{2-} (and / or OH^- ions in wet atmosphere). The apatite phase, being located at the grain boundaries of YDS and strongly bonded to the adjacent grains, would seem to play a key-role by creating diffusion short-circuits to the ionic species, between the grains.

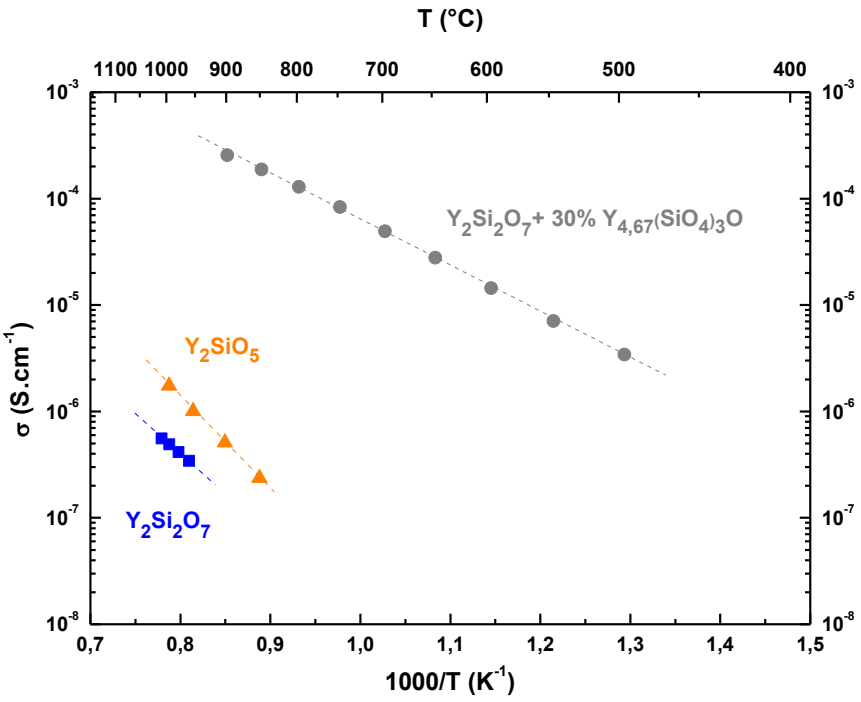

Figure 7: Arrhenius plots of the ionic conductivity measured by EIS of yttrium monosilicate, yttrium disilicate and a mix of yttrium disilicate and oxy-apatite yttrium with a similar relative porosity (6%) and grain size (around 5 µm), at high temperature under dry air (N_2/O_2=80/20)

3.3 Volatilization studies

Corrosion tests were carried out at high temperature (1400°C) in moist air (50 kPa of H_2O) under laminar flow (limitation by convection) with a gas velocity in hot zones of 28 $cm.s^{-1}$. The surfaces of pellets were mirror polished to get well defined and reproducible reactive surface areas.

Recession process of different silicate materials with similar microstructures

At 1400°C under moist air ($O_2/H_2O/N_2$ = 10/50/40 kPa, the volatilization kinetics for the yttrium disilicate and monosilicate shows a linear behavior over the first hours of corrosion (Figure 8). Monosilicate appears to be more resistant to volatilization phenomena in the presence of water vapor, with a thermochemical stability nearly 3 times higher than disilicate. This difference is much more noticeable than in previous works reported in the literature [12-14]. However, the possible dependence on the microstructure had not been taken in consideration in the previous works about the recession rate.

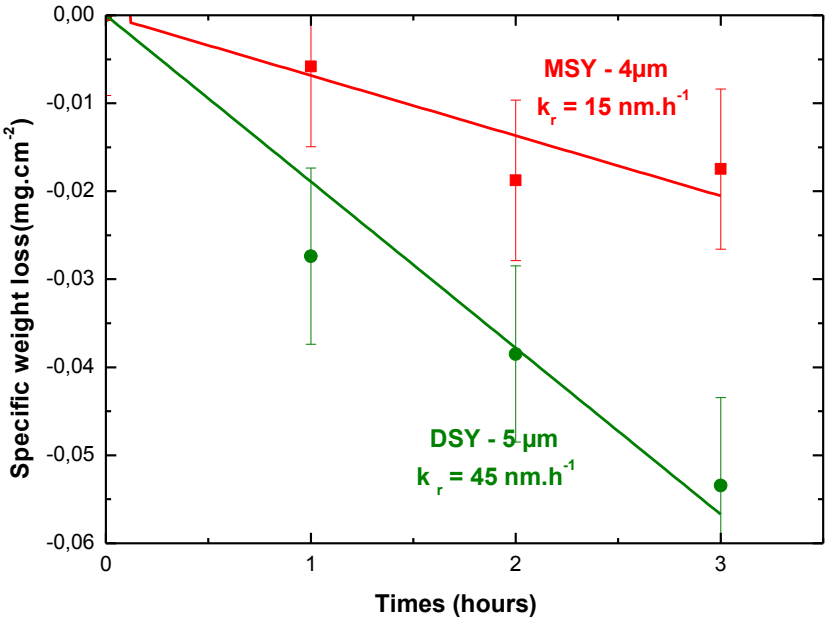

Figure 8: Specific weight loss of yttrium monosilicate and yttrium disilicate at 1400°C in moist air ($O_2/H_2O/N_2$ = 10/50/40 kPa), under laminar flow (limitation by convection) with a gas velocity in hot zones of 28 $cm.s^{-1}$

Recession process of disilicate materials with different microstructures

Corrosion tests were performed on materials with two grain sizes, Φ_{grain} ~ 0.8 and 4 µm, to establish a relation between the volatilization rate and the microstructure (Figure 9). The weight loss curves of these materials show a linear behavior over time and a constant volatilization rate could be extracted over the first hours of corrosion.

As much for mono as for disilicate, the decrease of grain size (by a factor of 5) lead to a neat rise in the values of recession rates (by a factor of 5) (Table 2). This rising of recession rate with the decrease of the gain sizes has been related to the higher grain boundary area fraction. Indeed, these latter areas are poorly crystallized and the attacks by corrosive species are much more localized there.

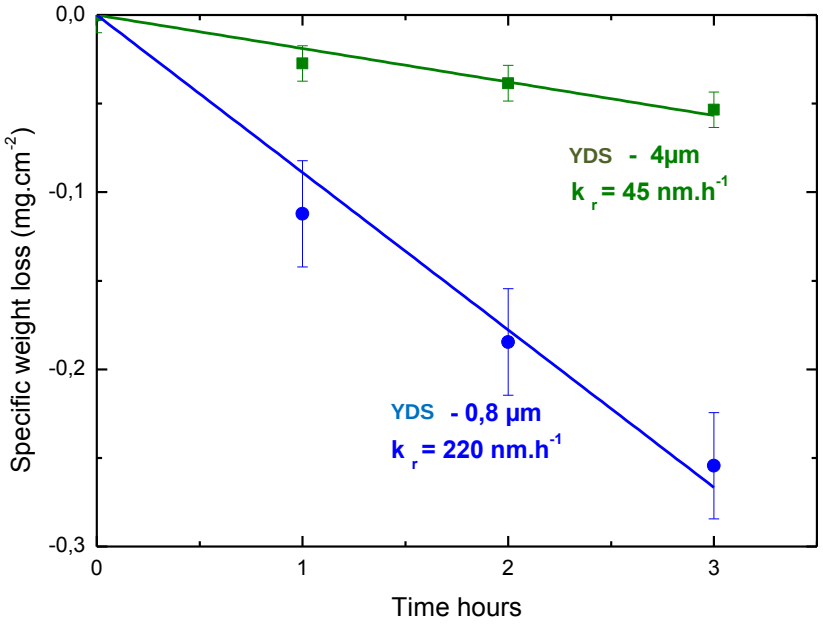

Figure 9: Specific weight loss of yttrium monosilicate and yttrium disilicate at 1400°C in moist air ($O_2/H_2O/N_2$ = 10/50/40 kPa), under laminar flow (limitation by convection) with a gas velocity in hot zones of 28 cm.s^{-1}

Tableau 2: Recession rates k_r of silicates and silica at 1400 ° C ($O_2/H_2O/N_2$ = 10/50/40 kPa) under laminar flow (limitation by convection) with gas velocities in hot zones of 28 $cm.s^{-1}$

Material	YMS	YMS	YDS	YDS	Silica
Grain size (µm)	0.8	5	0.8	5	-
Recession rate k_r ($nm.h^{-1}$)	70	15	220	45	(calculated and measured [59]) 150

Observation of corroded surfaces

To locally observe the corrosion process, the extreme surface topology of aged samples was characterized by Atomic Force Microscopy as is can be seen on Figure 10 for a YDS typical sample.

The development of roughness on AFM micrographs showed where microstructural degradation mainly occurs. The results were similar for mono and disilicate. The corrosion mechanism was preferentially localized along the grain boundaries and a grain size reduction is observed. After 3 hours of oxidation, the grain boundaries are well revealed on the corroded surface of the pellet. This observation was exacerbated after 6 and 12 hours of treatment. Fine and deep grooves were created in place of these grain boundaries and they reached more than 1 µm deep after 12 hours of corrosion at 1400°C in a moist air.

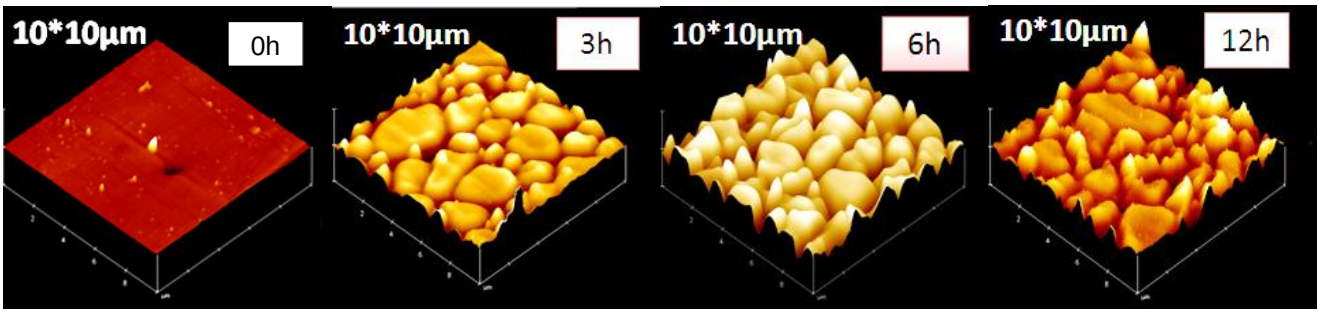

Figure 10: AFM images of yttrium disilicate surface before (0 hour) and after corrosion test (during 3, 6 and 12 hours) at 1400°C in moist air ($O_2/H_2O/N_2$ = 10/50/40 kPa), under laminar flow (limitation by convection) with a gas velocity in hot zones of 28 $cm.s^{-1}$

3.4 Oxidation of the silicon in the model coating

Since the bond coat for EBC on SiC/SiC composites is generally made of silicon, the corrosion tests on "sandwich"-type geometries are only done at 1300°C. On such a sample, the variation in weight measured is the result of two inverse contributions: matter lost from volatilization and weight gain from silicon oxidation. To focalize only on the oxidation/corrosion of silicon, the thickness of the silica scale is directly measured on a polished cross section of samples from micrographic observations for each aging time. To estimate the efficiency of protection of an EBC sample, the oxidation rates of silicon with an EBC and without (as-received) are compared using the same treatment.

Limitation of the oxidizing flow through an EBC in dry air

The evolution of the silica thickness versus time observed at 1300°C, in dry air, is reported on Figure 11. The oxidation kinetics for as-received silicon and coated silicon with a layer of YDS show a parabolic behavior, characterizing a passivation mechanism.

For as-received silicon samples, this kinetic of silica formation is characterized by a rapid growth of the SiO_2 layer, which is progressively reduced after 15 hours of treatment. The silica scale becomes protective (growth regime deviating from the linearity) when the silica thickness overcomes around $\delta_{SiO2} \sim 0.5$ µm. The oxidation of the underlying silicon can be considered being limited by the diffusion of oxygen across the silica scale.

In the case of silicon coated with yttrium disilicate, the mechanism appears similar. The slowing down of the oxidation speed is effective for a similar silica thickness close to $\delta_{SiO2} \sim 0.5$ µm. According to the lower oxygen flow across the EBC, the same thickness of silica is reached after 55 hours. To get this latter thickness, the growth mechanism is expected to be independent on the oxygen partial pressure in this short range of partial pressures.

During the first stage of oxidation, the interfacial growth rate can be considered as proportional to oxygen content at the silicon surface (the kinetic laws are commonly written with a relative order of reaction equal to 1 for oxygen) [60]. According to this hypothesis, the ratio between the initial slopes of the oxidation rates of these both silicon samples (0.036 and 0.0088 $\mu m.h^{-1}$) can be related to the limiting factor of the oxygen diffusion flow through the EBC layer (~ / 4). Respectively, the ratio between times required to reach a sufficient thickness of silica to move in a passive oxidation regime is similar (with inaccuracies close to the determination of this border). This ratio value is again found for any points in the parabolic regime between the instant growth rates for the same silica thickness (when this thickness is 0.8 µm, the local growth rates are respectively 0.016 ± 0.001 $\mu m.h^{-1}$ and 0.004 ± 0.001 $\mu m.h^{-1}$). Finally, the equivalent partial pressure of oxygen under this EBC, approximately 500 µm thick with a grain size of $\Phi_{grain} \sim 0.8$ µm, should be lowered to a value close to 5 kPa.

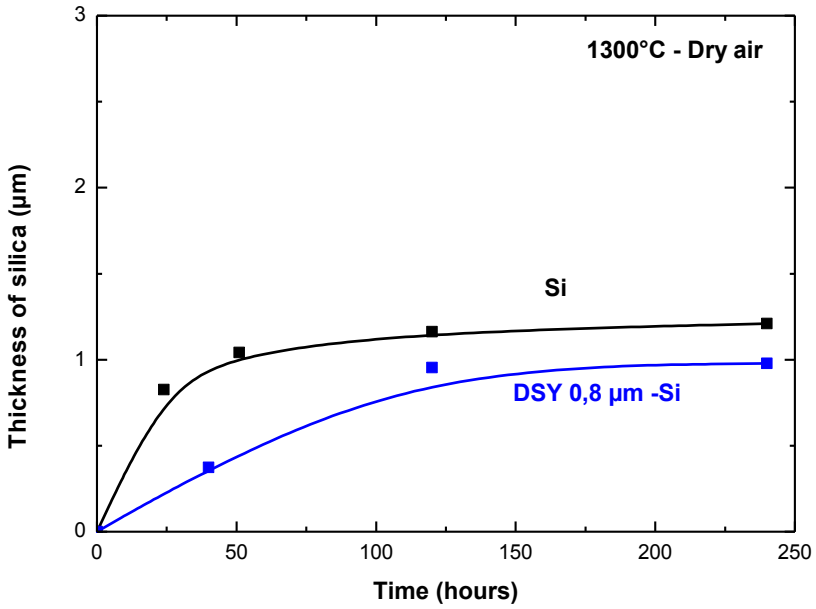

Figure 11: Kinetic oxidation (silica thickness versus time) of uncoated silicon and coated silicon with yttrium disilicate under dry air (O_2/N_2 = 20/80 kPa) at 1300°C, with a gas velocity in hot zones of 26 $cm.s^{-1}$

Limitation of the oxidizing flow through an EBC in moist air

The protection efficiency of an yttrium disilicate is expected to be related to the microstructure as previously shown by the conductivity measurements. Thus, measurements of the silica thicknesses formed at the EBC / Si interface were performed on "sandwich"-type samples made of EBC materials with different microstructures. Two sets of samples were made with either an average grain size of Φ_{grain} ~ 0.8 µm or 3 µm. The oxidation kinetics of silicon measured at 1300°C in wet air ($O_2/H_2O/N_2$ = 10/50/40 kPa) are shown on Figure 12. As a reference, the oxidation of as-received silicon is reported. But according to the volatilization of silica in presence of water vapor, the real formation rate of silica had to be calculated by summing at any time the thickness of residual silica and the equivalent one volatilized. This

calculation is based on a limitation of the volatilization through a diffusion across a boundary layer [61]: 0.023 µm.h^{-1}. The partial pressures of silicon hydroxide species are determined from [13-14]. Inversely, the volatilization of silica underneath the EBC coating is considered as negligible, due to its containment inside the sandwich architecture.

At 1300°C in such a moist environment, the shapes of the curves of silica growth on silicon are similar in any cases, with or without an EBC coating. The evolution of the thickness of the silica scale can be assumed as correctly described by a linear law. Such a behavior shows that the silica scale formed is not passivating, even for a thickness higher than 10µm at the DSY / Si interface.

The relative position of the curves in Figure 12 confirms that the microstructure and in particular the grain size has a significant influence on the oxidation protection of the Si substrate. Indeed, the coating with an average grain size of 3 µm seems to be less protective than the coating with submicronic grains. Following the same method of data analysis than previously, the increase of the grain size by a ratio around 3.75 lead to multiply the growth rate of the silica scale by a ratio close to 1.2 (≈ 0.024 µm.h^{-1} for a grain size equal to 0.8 µm and ≈ 0.028 µm.h^{-1} for 3 µm). This result is consistent with the evolution of ionic conductivity measurements in function of the grain size, (but with a lower ratio, in regard to measurements done under dry air).

Under wet atmosphere, the interfacial rate can be considered as proportional to water content at the silicon surface. The kinetic laws are commonly written with the relative orders of reaction equal to 1 for water and 0 for oxygen [60]. The respective growth rate of silica (residual + volatilized) on as-received silicon being equal to ≈ 0.048 µm.h^{-1}, the water diffusion flows up to silicon under the EBC are divided by a factor ~1.9 or 1.6 depending on the grain size (Φ_{grain} ≈ 0.8 or 3 µm). Finally, the equivalent partial pressure of water vapor under these EBC, approximately 500 µm thick, should be lowered to a value between ~26 kPa and 32 kPa.

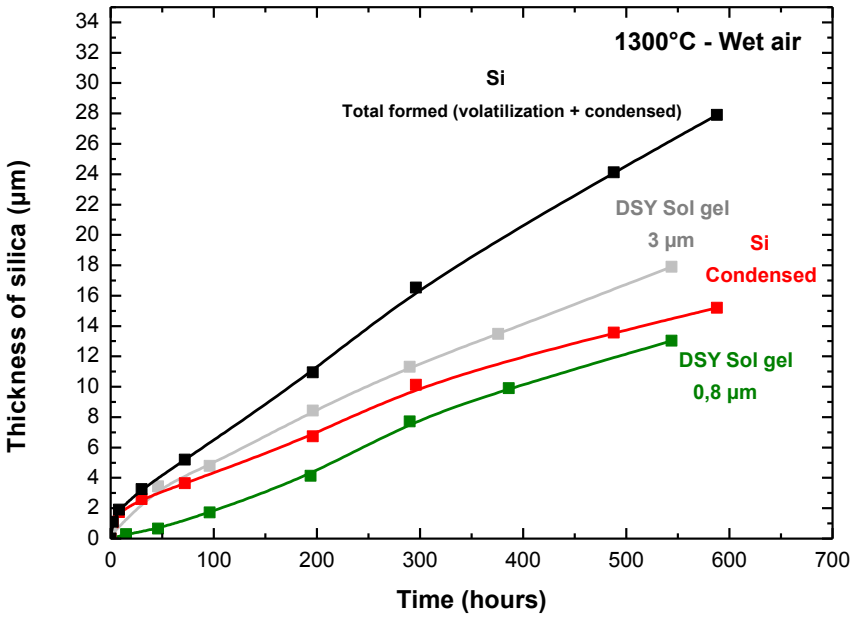

Figure 12: Kinetic oxidation of uncoated silicon and a coated silicon with yttrium disilicate with different microstructure at 1300°C in moist air ($O_2/H_2O/N_2$ = 10/50/40 kPa), under laminar flow (limitation by convection) with a gas velocity in hot zones of 28 $cm.s^{-1}$

Limitation of the oxidizing flow through different silicates in moist air

Following the same methodology, the protection efficiency of monosilicate is evaluated and compared to that of disilicate. On Figure 13, the kinetic of oxidation process are reported for sandwich samples with either YMS or YDS coatings. The relative position of the curves, YMS above YDS, is consistent with the classification of previously measured values of ionic conductivity for both samples: the monosilicate is less protective than the disilicate.

Under a monosilicate layer, the growth versus time of the silica scale can also be described by a linear law with a slope closer to that of the as-received silicon. For a same grain size of Φ_{grain} ~ 0.8 µm, this latter growth rate (≈ 0.043 µm.h^{-1}) is much higher than that under di-silicate: factor × 1.8.

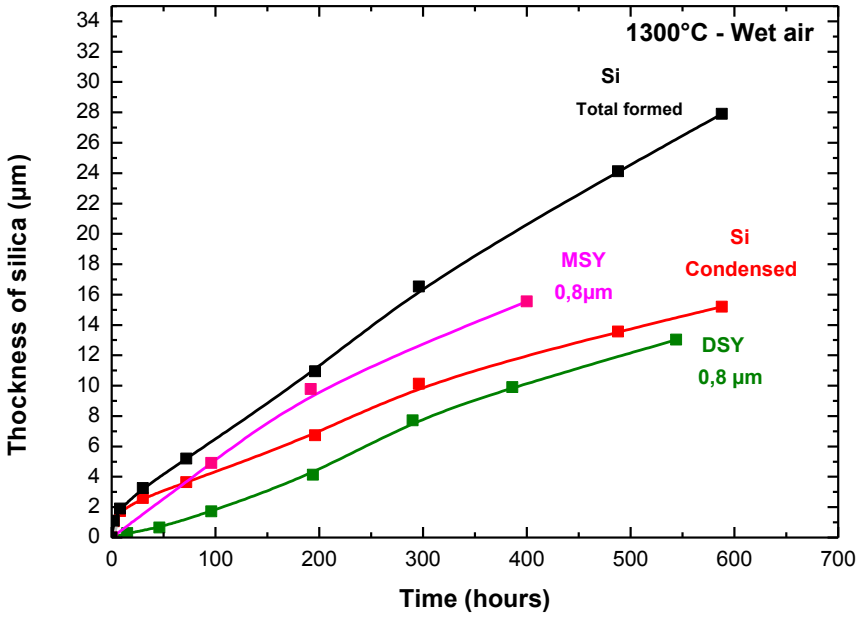

Figure 13: Kinetic oxidation behaviour of uncoated silicon and coated silicon with yttrium disilicate and silicon coated with yttrium monosilicate at 1300°C in moist air ($O_2/H_2O/N_2$ = 10/50/40 kPa), under laminar flow (limitation by convection) with a gas velocity in hot zones of 28 cm.s^{-1}

4- Discussion

4.1 Grain boundary and ionic conductivity

As discussed previously, the ionic conductivity of ceramic samples seems highly dependent on the amount of grain boundaries surface area. Thus, MET images of these regions have been performed on

yttrium silicate samples. The resolution point of the used apparatus (Philips CM30ST MET, with an acceleration voltage is 300 kV) is close to 0.2 nm. A typical example MET image observed on YDS pellets produced by natural sintering at 1400°C for 50 hours, is reported on Figure 14 in order to observe the boundaries microstructure. Analysis of these micrographs did not allow to identify polluting phases or glassy phases. According to the picture, the average thickness of the grain boundaries has been estimated at around 2 nm, which is a conventional value for such type of ceramic. As expected, no concordance of crystallographic arrangement is shown; a grain boundary becomes here a well-defined stop to ionic diffusion.

This blocking effect at the grain boundaries had already been shown in diverse oxides [33, 35, 37,59-65]. This effect is due to a variation of oxygen concentrations at the grain boundaries area. This chemical variation around a grain boundary could degrade locally the ionic conductivity. A high grain boundary density is therefore beneficial for reducing the ionic oxygen diffusion species within the structure of yttrium disilicate.

However, in an amorphous oxyde, a molecular diffusion can also take place, as mentionned during the oxidation of Si, through a vitreous silica scale [60].

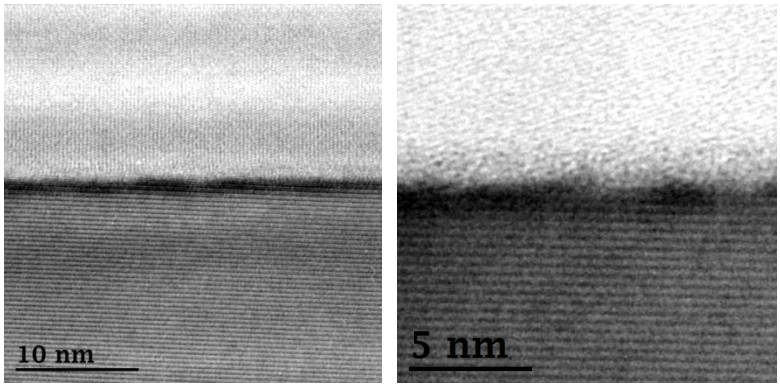

Figure 14: TEM images on the grain boundaries area between two grains of yttrium disilicate with different crystallographic orientations into a pellet produced by natural sintering at 1400°C for 50 h in air

4.2 Evolution of ionic conductivity in presence of water vapor

To better understand the influence of wet atmosphere on the ionic diffusion, additional conductivity measurements were carried out under different atmospheres (at atmospheric total pressure): dry air (O_2/N_2 = 20/80 kPa), moist air ($H_2O/O_2/N_2$ = 30/14/56 kPa) and wet nitrogen (H_2O/N_2 = 30/70 kPa). These gaseous mixtures allow to better identify or combine the effects of O^{2-} and OH^- on the ionic conductivity of YDS. The ionic conductivity measurements were carried out at 1100°C by time increments over 96 hours (humid air and wet nitrogen) or 24 hours (dry air) with conductivity measurements. These increments were respectively 5 hours (moist air, wet nitrogen) and 2 hours (air dry), up to reach stabilized measurements over time. All the measurements are reported on Figure 15.

In dry air, where only O^{2-} is the involved ionic species ($\sigma_{DRY} = \sigma_{O2-}$), the ionic conductivity seems to be very stable over time. Under wet nitrogen, the ionic conductivity increases significantly during more than 10 hours, before being constant. In that case, it can be considered that the only ionic species involved in the conduction process are OH^- ions ($\sigma_{WET\ N2} = \sigma_{OH-}$). Finally, it takes a little more time under moist air, with a continuous and regular much lower increase over time ($\sigma_{WET\ AIR}$).

Considering $\sigma_{WET\ N2}$, the initial increase in conductivity over 10 hours may be related to a progressive solubility of water into the disilicate with a formation of hydrates species in the structure. A saturation process into the crystallographic structure would then be shown through the stabilization of the ionic conductivity over time. The formation of these O-H bonds seems to further controlling the oxygen diffusion, since both curves in a moist environment have a similar initial shape. The hydroxyl anion OH^- is

known to be smaller than oxygen anion O^{2-}. This basic consideration could explain the larger OH^- mobility compared to O^{2-} (at least in the short time range).

Regarding the total ionic conductivity may be the sum of the ionic conductivities for each species, it can be deduced that the maximum hydration state could not be reached under wet air after 70 hours. Indeed, the experimental value is only $\sigma_{WET\ AIR} = 9 \times 10^{-6}$ S.cm^{-1} instead of $\sigma_{TOT} = 10 \times 10^{-6}$ S.cm^{-1} (as waited using the sum $\sigma_{TOT} = \sigma_{O2-} + \sigma_{OH-}$ in agreement with equation 5).

The increase of ionic conductivity is close to the simple ratio between the involved partial pressures of reactive species: when oxygen is replaced by water in the gaseous mixture, the ratio of partial pressures H_2O/O_2 is a factor of ~ 1.5 and the respective increase of conductivity is a factor ~1.3 ($\sigma_{O2-} = 4.7 \times 10^{-6}$ S.cm^{-1} and $\sigma_{OH-} = 5.95 \times 10^{-6}$ S.cm^{-1}). Inversely, the conductivity in moist air ($H_2O/O_2/N_2$ = 30/14/56 kPa) after 100 hours do not reached a value corresponding to the direct sum of that in wet nitrogen (H_2O/N_2 = 30/70 kPa) and in dry air (× 14/20): $\sigma_{TOT} = 9.24 \times 10^{-6}$ S.cm^{-1}. The overall increase in conductivity would appear as the sum of: the full contribution of water in the environment and the gradual contribution of oxygen ion diffusion over time, leading to a constant slow increase in the kinetic constant ($k_r = 2.7 \times 10^{-8}$ S.cm^{-1}.h^{-1}). In such a situation, 110 hours should be required to reach a stabilized state. With this first results, the modifications of ionic conductivity of a disilicate in oxidizing and corrosive environments begin to be predictable.

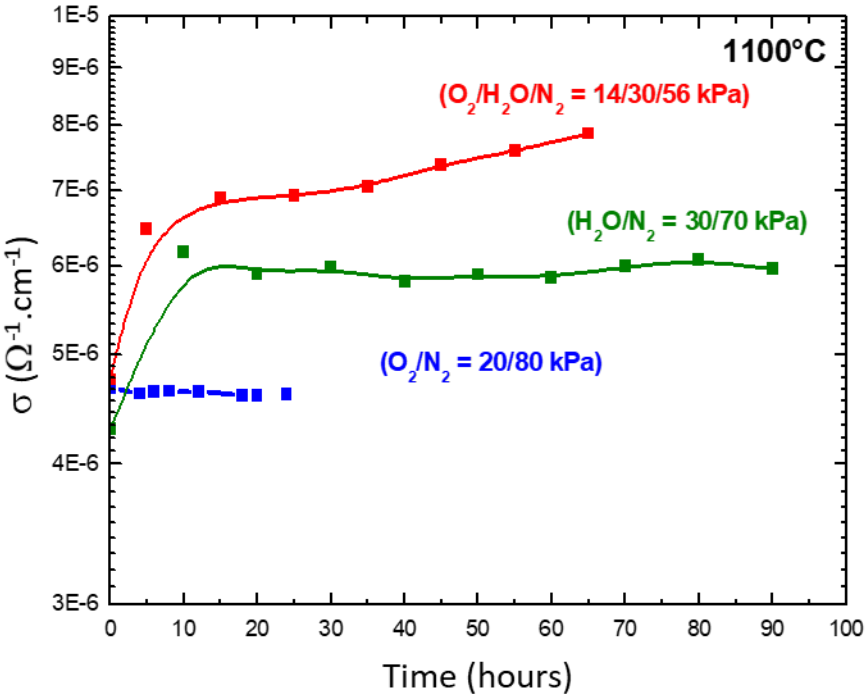

Figure 15: Ionic conductivity measured versus time by EIS measurements of yttrium disilicate, with a grain size of 5 µm at 1100°C in various gaseous mixtures.

4.3 Evolution of EBC properties with grain growth under working conditions

Under working conditions (temperature, pressure), the pieces undergo a heating treatment which can be responsible for sintering process with grain growth. Thus, the ionic conductivity of an initial dense EBC should increase over time at high temperature and certainly never decrease.

Furthermore, when the grain size is initially smaller (Φ_{grain} ~ 0.8 µm), a delay in the oxidation of the silicon pellet protected by the YDS can be observed in the "sandwich"-type geometry samples (Figures 12 and 13). As previously mentioned, the ionic conductivity, and respectively the ionic diffusion, is lowered with the increase of the surface area of grain boundaries. This behavior can be explained by two main phenomena:

- The first concerns the solubilization of oxidizing/corrosive species into the structure of the silicate material. This phenomenon can be identified according to the measurements of ionic conductivity in dry or wet air. Indeed, the material seems to hydrate initially, during at least 10 hours and therefore its O^{2-} ion or OH^- ion conduction properties increases over time.

- The second process may be explained by the morphological evolution of the ceramic sample (Figures 16-a, 16-b). Indeed, at 1300 °C under a high water partial pressure, water vapor can behave as a sintering agent. To demonstrate this hypothesis, a monitoring of the grain size as a function of time was carried out in similar corrosion conditions. The ceramic undergoes granular coalescence over time. This granular coalescence leads to an increase in grain size and therefore a decrease in the surface area of grain boundaries. To show the link between the microstructure and the conductivity during such experiments, values available of conductivity versus grain size are reported on Figure 16-c in the temperature range close to 1010°C. Considering small grain sizes (Φ_{grain} < 5µm), the increase of ionic conductivity can be considered, in a first approximation as proportional to the logarithm of the grain size. Thus, this evolution can be correctly represented by the relation (4):

$$Ln(\sigma) = 52{,}92.10^{-3} \times \Phi_{grain}^{\ 2} - 15{,}64 \qquad (4)$$

with d_g the grain average diameter in µm (the linear regression coefficient of the fitting is R^2 = 0.9915).

The ionic conductivity may significantly increase during aging. For example, for a coating at 1300°C, and after an ageing of 550 hours (Figure 16b), an increase of ionic conductivity is expected around 10% (if measured at 1010°C), in regard to equation (4). With the ageing of an EBC, made in disilicate, the diffusion of OH^- and O^{2-} ions could thus be expected to be progressively enhanced with the exponential of the square of the grain size. This trend of evolution has now to be considered in the analyses of the growth rate versus time of a TGO (thermal growth oxide by oxidation of the bonding layer) below the EBC.

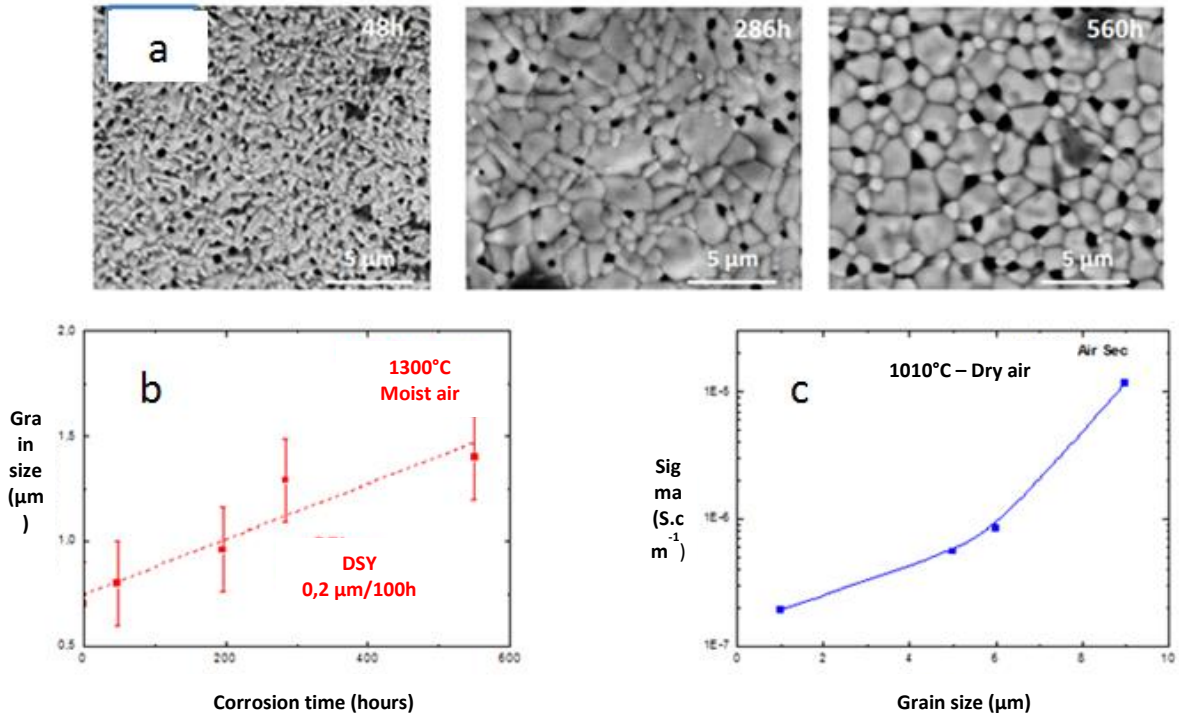

Figure 16: Corrosion test (evolution of the grain size versus time) on Yttrium disilicate in moist air ($O_2/H_2O/N_2$ = 10/50/40 kPa), under laminar flow (limitation by convection) with a gas velocity in hot zones of 28 $cm.s^{-1}$: (a) microstructural evolution over time at 1300°C, (b) Evolution of the grain size during corrosion at 1300°C and (c) illustration of the evolution of the ionic conductivity as a function of the grain size, measured at 1010°C.

It must be mentioned that the present results are in contradiction with diffusion properties observed by Wada et al [] with $Yb_2Si_2O_7$ ceramic using permeation measurements and ^{18}O isotopic exchange depth profiling by SIMS imaging. Indeed, this authors suggests that ultra-rapid oxide ions diffusion along the grain boundaries. This induces that a higher grain boundary density would result in a higher diffusivity. These apparent conflicting results could be explained by a difference of local grain boundary chemical composition (impurities) and also the thickness of the grain boundary and the width of the space charge area which can drastically modified the ionic diffusion behavior.

4.3 Diffusion coefficient extraction

To determine the effective oxygen diffusion coefficient within the coating, a recent accurate modelling have been previously proposed by Sullivan et al. [66, 67].

This model is developed in the case of a parabolic growth rate of the silica layer over the Si bond coat, met under dry air, at high temperature. In our case, in presence of moisture, with a high ratio of the total pressure, 50%, the growth rate of this layer can be assumed to be correctly described by a linear law, on the long ageing duration carried out, few hundred hours. A new modelling should be developed, based on a similar approach. Even if it appears simpler, it also considers the limited supply of oxidizing species by diffusion through the EBC layer up to the SiO_2 silica surface (Figure 18). The growth kinetic of a silica layer under an EBC was considered as proportional to the equivalent flux of H_2O, diffusing through the EBC and reaching the silicon surface. This scenario considers the contributions of two phenomena characterized by two linear constant rates versus time.

The effective rate constant of the TGO, ie. for an uncoated surface is defined as k ($m.s^{-1}$). It is the ratio between the incoming molar flux J_1 and the oxygen or water concentration at the surface C_{ext}:

$$J_1 = k.\ C_{ext} \qquad (5)$$

This rate constant is the linear rate of consumption of H_2O.

When the surface is coated by the EBC, one has an effective rate constant k_c defined in the same way:

$$J_2 = k_c . C_{ext} \quad (6)$$

Where J_2 is the new molar flux traversing the system consisting of the EBC and the TGO. At this stage, the limitation of the diffusion through the EBC is considered as a constant since its thickness is fixed and it is assumed to remain constant since the modification of microstructure is considered as insignificant during the duration of tests. This approach is proposed over a limited time of few hundred hours and is not affected by possible change of microstructures for longer aging times. This reasoning is based on the same flow equalities as those written by Deal and Grove or Sullivan (just adapted to a linear growth rate of the TGO). The relationship between k and k_c involves the diffusion coefficient through the EBC, as can be described using the following scheme (Figure 18):

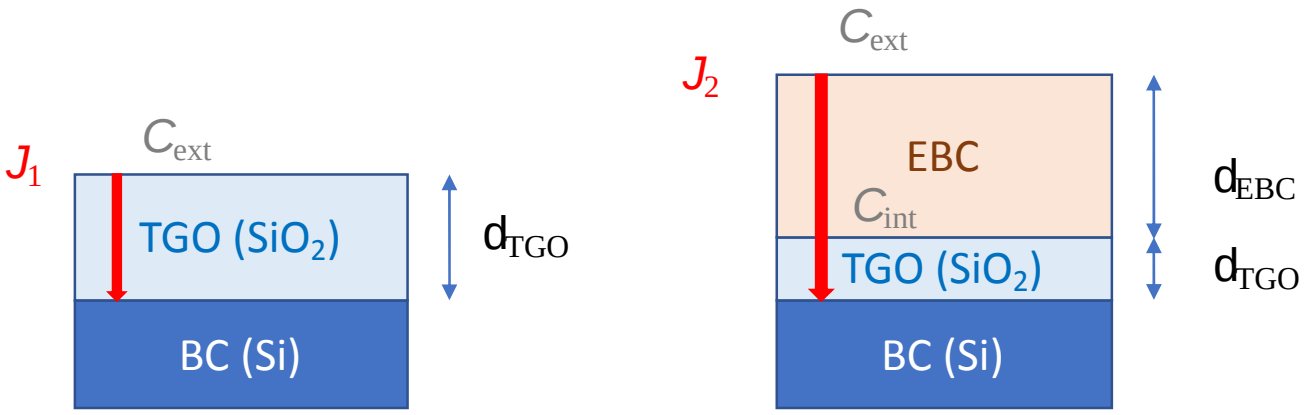

Figure 18: Schematic representation of the geometric models with and without an EBC. From the inside flows a value of effective diffusion coefficient can be extracted through an EBC, protecting a Si bond-coat (BC), with C_{ext} the concentration of the reactive species in the environment and C_{int} an equivalent concentration under the EBC

The flux J_2 can be written as :

$$J_2 = k. \times C_{int} \quad (7)$$

and as:

$$J_2 = (D_{EBC} / \delta_{EBC}) \times (C_{ext} - C_{int}) \quad (8)$$

Solving these two equations for C_{int} gives:

$$C_{int} = C_{ext} / (1 + k\delta_{EBC} / D_{EBC}) \quad (9)$$

So, we have:

$$J_2 = [k / (1 + k.\delta_{EBC} / D_{EBC})] \times C_{ext} \quad (10)$$

Or $$k_c^{-1} = k^{-1} + \delta_{EBC} / D_{EBC} \quad (11)$$

This relationship expresses the fact that the overall resistance to diffusion is the sum of two resistances in series, on linked to the TGO, the other one to the EBC. Reverting this expression gives:

$$D_{EBC} = \delta_{EBC} / (k_c^{-1} - k^{-1}) \quad (12)$$

These rate constants, k or k_c, are extracted from the slope (K) of linear fitting of the experimental values of silica thicknesses in function of time. This slope in $\mu m.h^{-1}$, has to be converted in $m.s^{-1}$, and progressively in number of moles of silica formed then number of moles of water consumed (twice) and divided by the concentration of water (C_{ext} = 3.82 $mol.m^{-3}$)

The relation is similar either for k or k_c, with K already converted in $m.s^{-1}$:

$$k_c = 2 \times K \times (\rho_{SiO2} / M_{SiO2}) / C_{ext} \quad (13)$$

with ρ_{SiO2} and M_{SiO2} respectively the density and the molecular mass of silica.

However, without an EBC, the whole thickness of silica formed, is the sum of the residual one and the one volatilized, (with a volatilization rate k_l, described earlier).

$$k = 2 \times (K + k_l) \times (\rho_{SiO2} / M_{SiO2}) / C_{ext} \quad (14)$$

All the extracted constant rates of silica growth are gathered in Table 3.

Table 3: constant rates of silica growth for Si without any coating around and in various EBC materials at 1300°C in moist air ($O_2/H_2O/N_2$ = 10/50/40 kPa).

	Si without any coating	Si coated with YDS grain size 0.8 µm (SPS sintering)	Si coated with YDS grain size 3 µm (SPS sintering)	Si coated with YMS grain size 0.8 µm (SPS sintering)
K in $m.s^{-1}$, in conditions of $C_{H2O(gas)}$ = 3.82 $mol.m^{-3}$	$(48 \pm 2) . 10^{-3}$	$(24 \pm 2) . 10^{-3}$	$(28 \pm 2) . 10^{-3}$	$(38 \pm 2) . 10^{-3}$
K in $mol.m^{-2}.s^{-1}$, in conditions of $C_{H2O(gas)}$ = 3.82 $mol.m^{-3}$	$(1.0 \pm 0,2) . 10^{-6}$	$(5.0 \pm 0,2) . 10^{-7}$	$(6.1 \pm 0,2) . 10^{-7}$	$(8.2 \pm 0,2) . 10^{-7}$
k for Si alone and k_c for Si coated with an EBC, in $m.s^{-1}$	$(2.6 \pm 0,2) . 10^{-7}$	$(1.3 \pm 0,2) . 10^{-7}$	$(1.6 \pm 0,2) . 10^{-7}$	$(2.1 \pm 0,2) . 10^{-7}$

The other way to quantify a diffusion coefficient through the EBC is the interpretation of EIS measurements. Indeed, the ionic conductivity and the diffusion coefficient are linked by the Nernst-Einstein equation, that can be written for each ionic species (see equation (15):

$$\sigma_i = \frac{D_i^{eff}{}_i z_i^2 e^2 C_i}{k_B T} \qquad (15)$$

With:

σ_i = partial ionic conductivity associated to species i ($S.cm^{-1}$)

z_i = effective charge of the species i (-2 for O^{2-} and -1 for OH^-)

e = elementary charge ($e = 1.602 \times 10^{-19}$ C)

C_i = concentration of the species i ($mol.cm^{-3}$).

D_i^{eff} = effective diffusion coefficient of species i ($cm^2.s^{-1}$)

k_B = Boltzmann constant ($k_B = 1.38 \times 10^{-23}$ J. K^{-1})

Since the inserted ionic concentration Ci in the crystallographic structure is unknown (as the Henry's law solubility coefficient for the oxidant in the oxide), all calculations of diffusion coefficient will again only be related to the concentration of the reactive species in the environment. Due to this configuration, the electrical conductivity σ_i is linked to an effective diffusion coefficient Di of species i by equation (15) (and not to the common ionic diffusion coefficient defined in the Nernst-Einstein equation). This consideration should introduce differences of values of diffusion coefficient with those obtained from isotope diffusion, given latter for comparison. As least, the trends about the impact of the nature of the silicate or the difference of microstructures should be conserved on these values.

Actually, the total ionic conductivity σ_{TOT} is the sum of the electrical conductivities of each species.

$$\sigma_{TOT} = \sum_i \sigma_i \qquad (16)$$

In moist air, two contributions in the ionic conductivity are expected: O^{2-} and OH^-, as opposed to corrosion tests in which a major species is responsible to the oxidation rate (reaction order different for each species). So, the values of effective diffusion coefficients extracted from equation (15) remain macroscopic since the only available value of concentration, C_i, is into the supplied reactive gas mixture (as done also in corrosion test when equation (10) is used).

For example, from the Figure 15, in a moist air, the values of conductivity for OH^- and O^{2-} ions can be easily extracted using equation (14). These values similar are similar, as already reported in part 4.2.

Contrary, the values of effective diffusion coefficients, calculated using equation 11, highlight that OH^- ion is more mobile than O^{2-} ion in yttrium disilicate (with a grain size of $\Phi_{grain} \sim 5$ µm): $D_{O^{2-}} = (8.2 \pm 0.2) \times 10^{-13}\ m^2.s^{-1}$ (dry air environment) and $D_{OH^-} = (2.7 \pm 0.1) \times 10^{-12}\ m^2.s^{-1}$ (wet nitrogen environment), at 1100°C ($D_{OH^-} > 3 \times D_{O^{2-}}$).

Respectively, the values of efficient ionic diffusion coefficients evolve as the ionic conductivity versus the grain size (Table 4). Such an evolution may occur during the ageing of an EBC, as shown on Figure 16c.

Then, it becomes possible to compare the calculated effective diffusion coefficient (see equation (15) from ionic conductivity measurements performed with EIS with the effective coefficient of diffusion extracted from the gas fluxes (see equation (12)) required to TGO growth kinetics.

The results are reported in Table 4, with the surrounding partial pressures of oxidizing or corrosive species. The main oxidizing species are expected to be hydroxyl ion OH^- in wet atmosphere [3, 4, 60]. As the only accessible values are the partial pressures of reactive species, the extracted diffusion coefficient, calculated from the partial pressures of oxidizing or corrosive species (dry or wet environment), are effective values, as commonly considered in the oxidation kinetic laws of Si or SiC [3, 4, 60].

Considering the dry oxygen atmosphere and YMS, YDS and ytterbium disilicate materials and whatever the particle size, it can be noticed that all calculated diffusion coefficients from ionic conductivity measurements are close. Nevertheless, that determined for $Y_2Si_2O_7$ is as expected higher. It can be concluded that the protection provided by ytterbium disilicate is more efficient than yttrium disilicate [68]. A comparing with values of diffusion coefficient obtained from the isotopic exchange method can be done but by keeping in mind that the diffusion driving force may be different. During the isotopic exchange process, the involved gradient in the calculation of diffusion coefficient is only function of the tracer $^{18}O^{2-}$ species inserted in the crystalline structure. Considering the corrosion tests, a gradient of

oxygen activity into the solid phase has to be considered as driving force (consumption by the oxidation of the Si bond coat). Elsewhere, the value extracted from tracer diffusion experiments on single-crystal gives much lower values of effective diffusion coefficient. However, a single-crystal only involves bulk diffusion processes and should induce a reduced concentration of defects. In summary, the effective diffusion coefficient calculation takes only into account a gradient of dissolved $^{18}O^{2-}$ ion concentration into the ideal crystalline network. Further, the inserted amount of the tracer $^{18}O^{2-}$ at the top surface of the oxide is well known and allows extracting an intrinsic value of coefficient (this amount of tracer substituted into the crystalline structure is much smaller than the partial pressure $^{18}O_2$). Unfortunately, this latter value is the not available in our proposed and the extraction of effective diffusion coefficient is only possible (equations (5) to (14) and (15)). Thus, our estimations are based on equivalent ion concentrations, regarding the oxygen and/or water partial pressures.

Another hypothesis to this difference may be that the diffusion through the EBC has two main contributions: (i) ionic in the crystalline network and (ii) molecular through the grain boundaries. In oxide materials, these boundaries areas are often described to act as diffusion short-circuits of molecular diffusion [40, 51, 69, 70, 49] since an amorphous oxide offers a potential pathway to molecular diffusion [60] (the same zone can act simultaneously as a barrier against ionic diffusion).

Despite this difference of level between calculated values, and considering the independence of the methods and the respective approximations into calculation, the global trends of evolution of diffusion coefficients are in good agreement (Table 4).

This work shows that an yttrium monosilicate has a coefficient of diffusion at least, one order of magnitude higher than that of a disilicate. So, YMS is clearly less efficient into an EBC to limit the oxidative/corrosive species diffusion. YbMS

Our work has also to be compared to results on YbDS and YbMS that mention a preferential diffusion along grain boundaries [40, 71]. It was found that the more preferentially an oxide ion diffuses in the grain boundary compared to the interior of the grain, the greater the effect of suppressing the movement of the oxide ion by applying an oxygen potential gradient becomes. It has been shown that oxygen permeation proceeded via mutual diffusion of oxide and Yb ions at the grain boundaries with a large contribution from oxide ions. with the introduction of H_2O to O_2, the interdiffusion of oxide and Yb ions was accelerated, but no oxygen permeation was detected [40, 72]. YbDS is known to have a different crystalline structure [29] and consequently may possess properties of mass transfer, as different oxygen lattice and grain boundary diffusion coefficient. Anyway, O_2 and H_2O molecular forms may diffuse within the cracks or grain boundaries but also in dense materials in ionic forms according to the migration of O^{2-} and OH^- anions in the crystalline network of the material.

In summary, in regard to Wada' works [40, 70, 71], the method of Electrochemical Impedance Spectroscopy allows only to characterize the mobility of ionic species [34-37], and allows to extract only one contribution involved into the oxidizing/corrosive species diffusion. In comparison, the values of diffusion coefficient extracted from experimental measurements of silica thicknesses involves both diffusion modes. In our case, the increase of density of grain boundaries seems to slow down the diffusion but the evolution of the width of the grain boundary in regard to their density (or the grain growth) is not considered here.

Table 4: Calculated effective diffusion coefficient of oxygen and water in various EBC materials at high temperature under atmospheric pressure, from ageing of "sandwich"-type samples.

	SiO_2	Mullite single	YMS single	YDS (Plasma	Ytterbium disilicate	YDS grain size 0.8	YDS grain size 3	YMS grain size

		crystal-line	crystalline	spray)	(Plasma spray)	µm (SPS sin-tering)	µm (SPS sintering)	0.8 µm (SPS sintering)
D_O^{2-} $m^2.s^{-1}$ in dry air	1300°C $3.3\ 10^{-23}$ [73]	1250°C $1\ 10^{-20}$ [38]	1300°C $(6.00 \pm 0.01)\ 10^{-18}$ [45]					
D_{OH^-} $m^2.s^{-1}$, in a wet air	1200°C $4.8\ 10^{-12}$ [45].			1300°C $(2,8 \pm 1,1)\ .\ 10^{-11}$ m²/s For $C_{H2O(gas)}$ =6.88 $mol.m^{-3}$ [69]	1300°C $2,03\ 10^{-12}$ [74]	1300°C $(1,3 \pm 0.3)\ .\ 10^{-10}$ This work, for $C_{H2O(gas)}$ = 3.82 $mol.m^{-3}$	1300°C $(2,0 \pm 0.3)\ .\ 10^{-10}$ This work, for $C_{H2O(gas)}$ = 3.82 $mol.m^{-3}$	1300°C $(5,9 \pm 0,3)\ .\ 10^{-10}$ This work, for $C_{H2O(gas)}$ = 3.82 $mol.m^{-3}$
Calculated D_O^{2-}, m²/s, from ionic conductivi-ty in dry air						At 1300°C, $(4.6 \pm 0.2)\ .\ 10^{-13}$ This work, for $C_{O2(gas)}$ = 1.53 $mol.m^{-3}$	At 1300°C, $(1.1 \pm 0.2)\ .\ 10^{-12}$ This work, for $C_{O2(gas)}$ = 1.53 $mol.m^{-3}$	At 1300°C, $(7 \pm 2)\ .\ 10^{-12}$ This work, for $C_{O2(gas)}$ = 1.53 $mol.m^{-3}$

5 - Conclusion

In the field of Environmental Barrier materials, this work is dedicated to the development of new compounds and an original methodology to study the effect of the microstructure on the essential properties of the specifications of an EBC: ionic conductivity, the diffusion of oxidizing species, the kinetics of growth of the silica layer, the material recession rate. Several new specific approaches were proposed: the electrochemical impedance spectroscopy to access to the ionic conductivity, model samples using a

sandwich-type geometry to extract global diffusion coefficient across EBC and corrosion tests of polished surfaces to localize the corrosion.

The different measurements of ionic conductivity under dry air made possible to propose a classification of silicates with respect to their ionic transport properties of oxidizing species. It appears that yttrium oxy-apatite shows a relatively good ionic conductor and therefore by definition a less efficient material as an environmental barrier. Yttrium disilicate is more effective as an EBC material than monosilicate. Moreover, the increased surface area of the grain boundaries contributes to a decrease in the ionic conductivity of the ceramic samples. A submicronic microstructure is therefore more favorable than a microstructure with a large grain size.

The effect of grain boundaries on recession seems to be inverse. Due to their lower degree of crystallization, corrosion starts along these regions and further, recession occurs deeper inside these boundaries. The present study shows that monosilicate present a better stability under corrosion and recession conditions than yttrium disilicate.

The development of “sandwich”-type geometries ceramic samples with dense coatings allows to get model sample to quickly compare selected EBC materials. The analysis of the silica growth under the EBC layer allows determining a global diffusion coefficient either oxygen or water depending on the composition of the gaseous environment at high temperature. The evolution of these latter diffusion coefficients could be compared to ionic conductivity measurements versus temperature, nature of the silicate and microstructure. The same trends are found in function of these environmental parameters. The calculations of diffusion coefficient from these different measurements are themselves consistent and in agreement with the literature. This methodology confirms that the measurement of the ionic conductivity can be a relevant parameter for characterizing the protection of a material facing the diffusion of oxidizing species.

These results provide a rich database on yttrium silicates and help to better understand the influence of microstructure on material performance. In addition, the present study is the starting point for optimizing the composition of rare earth disilicates in order to optimize their performance (retain and preservation of the microstructure during a corrosion test).

However, to extrapolate these results to working conditions of aeronautical turbines with much higher gas speeds (several hundred $m.s^{-1}$), it will be then necessary to get data in high gas flow rate conditions; modifications of the phenomena of volatilization and therefore of material recession may occur.

The hypothesis that oxidation rate of silicon under an EBC keeps proportional with oxidizing/corrosive gaseous concentration has to be checked in future study. Many experiments under various gas mixtures at different temperatures have to be now carried out.

These results demonstrate that to obtain the best protection against the diffusion of ionic species and the lowest volatilization rate of the material, a combination between the natures of silicates and their microstructures must be considered. Thus, the EBC must be processed with a multilayered architecture where each layer has its own functionality. The optimal architecture should possess gradients of composition and microstructure from the surface to the bulk as reported on Figure 19.

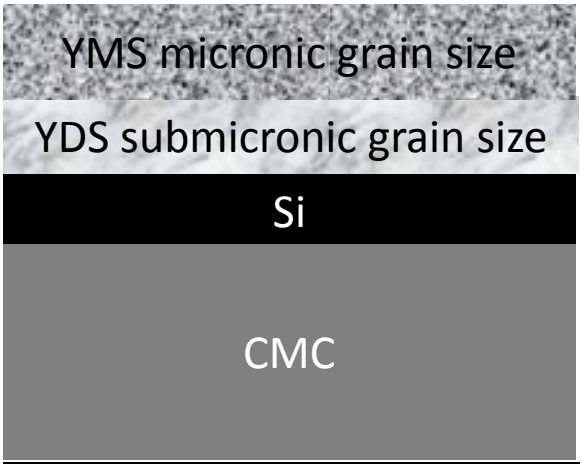

Figure 19: Schematic of an optimised EBC with a gradient of microstructure:

The external layer should be made of a monosilicate with a large grain size to limit volatilization. In addition, its low thermal conduction coefficient allows also getting a function as Thermal Barrier Coating (TBC). The temperature of the second layer should be lowered and thermochemically activated physicochemical phenomena such as granular coalescence or species diffusion in ionic form will be limited. The second layer is made of a submicronic yttrium disilicate layer. It is selected to act as a diffusion barrier. Thus, the decrease of the diffusion flow through the EBC limit the oxidation of the silicon bonding layer.

Acknowledgements

The authors would like to thank Safran Ceramics for grant associated to this work and many engineers from Safran, L. Pin, E. Courcot-Mendez and E. Bouillon for fruitful discussions.

References

[1] I. Spitsberg, J. Steibel, “Thermal and environmental barrier coatings for SiC/SiC CMCs in aircraft engine applications”, International Journal of Applied Ceramic Technology. 1 (4) 2004. p. 291-301.

[2] K. Rebstock, “Reliability protection systems for ceramic matrix composites”, Protective coatings and thin films. Ed. Y. Pauleau, P.B. Barna. 1997. p. 511-522.

[3] E.J. Opila, “Variation of the Oxidation Rate of Silicon Carbide with Water-Vapor Pressure”, J. Am .Ceram. Soc., 82 [3], pp. 625-36, 1999. https://doi-org.inc.bib.cnrs.fr/10.1111/j.1151-2916.1999.tb01810.x

[4] E.J. Opila, “Oxidation and volatilization of silica formers in water vapor”, J. Am. Ceram. Soc., 86 [8], pp. 1238-48, 2003. https://doi-org.inc.bib.cnrs.fr/10.1111/j.1151-2916.2003.tb03458.x

[5] K.N. Lee, “Current status of environmental barrier coatings for Si-based ceramics”, Surf. Coat. Technol., 133-134, pp. 1-7, 2000. https://doi.org/10.1016/S0257-8972(00)00889-6

[6] M. Aparicio and A. Durán, “Yttrium silicate coatings for oxidation protection of carbon-silicon carbide composites”, J. Am. Ceram. Soc., 83 [6], pp. 1351–1355, 2000. https://doi-org.inc.bib.cnrs.fr/10.1111/j.1151-2916.2000.tb01392.x

[7] Z. Sun, J. Wang, M. Li, and Y. Zhou, “Mechanical properties and damage tolerance of Y_2SiO_5”, J. Eur. Ceram. Soc., 28 [15], pp. 2895–2901, 2008. https://doi.org/10.1016/j.jeurceramsoc.2008.04.029

[8] Z. Tian, X. Ren, Y. Lei, L. Zheng, W. Geng, J. Zhang, and J. Wang, “Corrosion of $RE_2Si_2O_7$ (RE=Y, Yb, and Lu) environmental barrier coating materials by molten calcium-magnesium-

alumino-silicate glass at high temperatures", J. Eur. Ceram. Soc., 39 [14], pp. 4245–4254, 2019. https://doi.org/10.1016/j.jeurceramsoc.2019.05.036

[9] Z. Tian, L. Zheng, J. Wang, P. Wan, J. Li, and J. Wang, "Theoretical and experimental determination of the major thermo-mechanical properties of RE_2SiO_5 (RE = Tb, Dy, Ho, Er, Tm, Yb, Lu, and Y) for environmental and thermal barrier coating applications", J. Eur. Ceram. Soc., 36 [1], pp. 189–202, 2016. https://doi.org/10.1016/j.jeurceramsoc.2015.09.013

[8] Z. Tian, L. Zheng, Z. Li, J. Li, and J. Wang, "Exploration of the low thermal conductivities of γ-$Y_2Si_2O_7$, b-$Y_2Si_2O_7$, β-$Yb_2Si_2O_7$, and β-$Lu_2Si_2O_7$ as novel environmental barrier coating candidates", J. Eur. Ceram. Soc., 36 [11], pp. 2813–2823, 2016. https://doi.org/10.1016/j.jeurceramsoc.2016.04.022

[10] Z. Sun, Y. Zhou, J. Wang, and M. Li, "Thermal properties and thermal shock resistance of γ-$Y_2Si_2O_7$", J. Am. Ceram. Soc., 91(8], pp. 2623–2629, 2008. https://doi.org/10.1111/j.1551-2916.2008.02470.x.

[11] Z. Sun, Y. Zhou, J. Wang, and M. Li, "γ-$Y_2Si_2O_7$, a machinable silicate ceramic: Mechanical properties and machinability", J. Am. Ceram. Soc., 90 [8], pp. 2535–2541, 2007. https://doi.org/10.1111/j.1551-2916.2007.01803.x.

[12] E. Courcot, F. Rebillat, F. Teyssandier, C. Louchet-Pouillerie, "Thermochemical stability of the Y_2O_3–SiO_2 system", J. Eur. Ceram. Soc., 30 [9], pp. 905-910, 2010, https://doi.org/10.1016/j.jeurceramsoc.2009.09.007

[13] E. Courcot., F. Rebillat, F. Teyssandier, C. Louchet-Pouillerie, "Stability of rare earth oxides in a moist environment at high temperatures-Experimental and thermodynamic studies. Part I: The way to assess thermodynamic parameters from volatilisation rates", J. Eur. Ceram. Soc., 30 [9],

pp. 1903-1909, 2010. https://doi.org/10.1016/j.jeurceramsoc.2010.02.011

[14] E. Courcot, F. Rebillat, F. Teyssandier, C. Louchet-Pouillerie, "Stability of rare earth oxides in a moist environment at elevated temperatures-Experimental and thermodynamic studies. Part II: Comparison of the rare earth oxides", J. Eur. Ceram. Soc., 30 [9], pp. 1911-1917, 2010, https://DOI: 10.1016/j.jeurceramsoc.2010.02.012

[15] J. F. Huang, H. J. Li, X. R. Zeng, and K. Z. Li, "Yttrium silicate oxidation protective coating for SiC coated carbon/carbon composites", Ceram. Int., 32 [4], pp. 417–421, 2006. https://doi:/10.1016/j.ceramic int.2005.03.018

[16] I. A. Bondar, "Rare-Earth Silicates", Ceram. Int., 8 [3], pp. 83–89, 1982, https://doi.org/10.1016/0272-8842(82)90022-0

[17] J. Felsche, "The Crystal Chemistry of the Rare-Earth Silicates", Structure and Bonding, Springer, Berlin, Heidelberg, 13, pp. 99–197, 1973, https://doi.org/10.1007/3-540-06125-8_3

[18] B. Liu, J. Wang, F. Li, J. Wang, and Y. Zhou, "Mechanisms of Mono-Vacancy and Oxygen Permeability in Y_2SiO_5 Orthosilicate Studied by First-Principles Calculations", J. Am. Ceram. Soc., 95 [3], pp. 1093–1099, 2012. https://doi-org.inc.bib.cnrs.fr/10.1111/j.1551-2916.2011.05046.x

[19] S. Kumar and C. H. Drummond, "Crystallization of various compositions in the Y_2O_3-SiO_2 system", J. Mater. Res., 7 [4], pp. 997–1003. https://doi-org.inc.bib.cnrs.fr/10.1557/JMR.1992.0997

[20] D.L. Poerschke, D.D. Hass, S. Eustis, G.G.E. Seward, J.S. Van Sluytman, and C.G. Levi, "Stability and cmas resistance of ytterbium-silicate/hafnate EBCS/TBC for SiC composites", J. Am. Ceram. Soc., 98 [1], pp. 278–286, 2015. https://doi.org/10.1111/jace.13262

[21] D.L. Poerschke, R.W. Jackson, and C.G. Levy, "Silicate deposit degradation of engineered coatings in gas turbines: Progress toward models and materials solutions", Annual Review of Materials Research, 47, pp. 297–330, 2017. https://doi.org/10.1146/annurev-matsci-010917-10500

[22] D.L. Poerschke, J.H. Shaw, N. Verma, F.W. Zok, and C.G. Levi, "Interaction of yttrium disilicate environmental barrier coatings with calcium-magnesium-iron alumino-silicate melts", Acta Materialia, 145, pp. 451–461, 2018. https://doi.org/10.1016/j.actamat.2017.12.004

[23] W.D. Summers, D.L. Poerschke, M.R. Begley, C.G. Levi, and F.W. Zok, "A computational modeling framework for reaction and failure of environmental barrier coatings under silicate deposits", J. Am. Ceram. Soc., 103 [9], pp. 5196–5213, 2020. https://doi.org/10.1111/jace.17187

[24] W.D. Summers, D.L. Poerschke, D. Park, J.H. Shaw, F.W. Zok, and C.G. Levi, "Roles of composition and temperature in silicate deposit-induced recession of yttrium disilicate", Acta Materialia, 160, pp. 34–46, 2018. https://doi.org/10.1016/j.actamat.2018.08.043

[25] W.D. Summers, D.L. Poerschke, A.A. Taylor, A.R. Ericks, C.G. Levi, and F.W. Zok, "Reactions of molten silicate deposits with yttrium monosilicate", J. Am. Ceram. Soc., 103 [4], pp. 2919–2932, 2020. https://doi.org/10.1111/jace.16972

[26] J. Felsche, W. Hirsiger, "The polymorphs of the rare-earth pyrosilicates R.E.$_2$Si$_2$O$_7$, [R.E.: La, Ce, Pr, Nd, Sm]", J. of the Less-Comm Metals, 131 [18], pp. 131–137, 1969. https://doi.org/10.1016/0022-5088(69)90132-5

[27] M. Marezio, J. P. Remeika, and P. D. Dernier, "The crystal chemistry of the rare earth orthoferrites", Acta Crystallogr. Sect. B Struct. Crystallogr. Cryst. Chem., 26 [12] pp. 2008–2022, 1970. https://doi.org/10.1107/S0567740870005319

[28] N. A. Toropov, V. P. Barzakovskii, I. I. Bondar, P. Yu, Udalov, "Phase diagrams of silicate sys-

tems", Reference book, 2, Metal-oxygen compounds of silicate systems," 1970.

[29] T. Warshaw, R. Roy, "Polymorphism of the rare earth sesquioxides", J. Phys. Chem. 65, pp. 2048, 1961. https://doi-org.inc.bib.cnrs.fr/10.1021/j100828a030

[30] J. Felsche, "Rare Earth Silicates with the Apatite Structure", J. Solid State Chem, 5 [2], pp. 266–275, 1972. https://doi.org/10.1016/0022-4596(72)90039-4

[31] P. J. Panteix, E. Béchade, I. Julien, P. Abélard, D.Bernache-Assollant, "Influence of anionic vacancies on the ionic conductivity of silicated rare earth apatites", Mat. Res. Bull., 43, pp. 1223–1231, 2008. https://doi.org/10.1016/j.materresbull.2007.05.030

[32] K. Kobayashi, Y. Sakka, "Rudimental research progress of rare-earth silicate oxyapatites : their identification as a new compound until discovery of their oxygen ion conductivity", J. of Ceram. Soc. of Japan, 122 [8], pp. 649–663, 2014. https://doi.org/10.2109/jcersj2.122.649

[33] D. Marrero-López, L. Dos Santos-Gómez, L. León-Reina, J. Canales-Vázquez, E. R. Losilla, "Influence of the microstructure on the bulk and grain boundary conductivity in apatite-type electrolytes", J. Power Sources, 245, pp. 107–118, 2014. https://doi.org/10.1016/j.jpowsour.2013.06.111

[34] N. Bonanos, R. K. Slotwinski, B. C. H. Steele, E. P. Butler, "High ionic conductivity in polycrystalline tetragonal Y_2O_3-ZrO_2", J. Mater. Sci. Lett., 3 [3], pp. 245–248, 1984. https://doi-org.inc.bib.cnrs.fr/10.1007/BF00726805

[35] J. M. Porras-Vázquez, E. R. Losilla, L. León-Reina, D. Marrero-López, M. A. G. Aranda, "Microstructure and oxide ion conductivity in a dense $La_{9.33}(SiO_4)_6O_2$ Oxy-Apatite", J. Am. Ceram. Soc., 92 [5], pp. 1062–1068, 2009. https://doi-org.inc.bib.cnrs.fr/10.1111/j.1551-2916.2009.03032.x

[36] C. Peters, A. Weber, B. Butz, D. Gerthsen, and E. Ivers-Tiffée, "Grain-size effects in YSZ thin-film electrolytes", J. Am. Ceram. Soc., 92 [9], pp. 2017–2024, 2009. https://doi-org.inc.bib.cnrs.fr/10.1111/j.1551-2916.2009.03157.x

[37] B. Wang, Z. Lin, "A Schottky barrier based model for the grain size effect on oxygen ion conductivity of acceptor-doped ZrO_2 and CeO_2", Int. J. Hydrogen Energy, 39 [26], pp. 14334–14341, 2014. https://doi.org/10.1016/j.ijhydene.2014.03.142

[38] P. Fielitz, G. Borchardt, M. Schmücker, H. Schneider, M. Wiedenbeck, D. Rhede, S. Weber, S. Scherrer, "Secondary Ion Mass Spectroscopy of Oxygen-18 Tracer Diffusion in 2/1-Mullite Single Crystals", J. Am. Ceram. Soc., 84[12], pp. 2845–2848, 2001. https://doi-org.inc.bib.cnrs.fr/10.1111/j.1151-2916.2001.tb01103.x

[39] J. C. Mikkleson, "Self-Diffusivity of Network Oxygen in Vitreous SiO_2", Appl. Phys. Lett., 45 [11], pp. 1187-1189, 1984. https://doi.org/10.1063/1.95086

[40] M Wada, T. Matsudaira, N. Kawashima, S. Kitaoka, M. Takata, "Mass transfer in polycrystalline ytterbium disilicate under oxygen potential gradients at high temperatures", Acta Materialia, 135, pp. 372-381, 2017. https://doi.org/10.1016/j.actamat.2017.06.029

[41] T. Iwata, K. Fukuda, E. Béchade, O. Masson, I. Julien, E. Champion, "Structural change of oxide-ion-conducting lanthanum silicate on heating from 295 to 1073 K", Solid State Ionics, 178 [27-28], pp. 1523–1529, 2007. https://doi.org/10.1016/j.ssi.2007.09.006

[42] R. A. De Souza, J.A. Kilner, "Oxygen transport in $La_{1-x}SrxMn_{1-y}CoyO_{3\pm\delta}$ perovskites Part I. Oxygen tracer diffusion", Solid State Ionics, 106 [3–4], pp. 175–187, 1998. https://doi.org/10.1016/S0167-2738(97)00499-2

[43] E. Boehm, J. M. Bassat, P. Dordor, F. Mauvy, J. C. Grenier, and P. Stevens, "Oxygen diffusion

and transport properties in non-stoichiometric $Ln_{2-X}NiO_{4+\delta}$ oxides", Solid State Ionics, 176 [37–38], pp. 2717–2725, 2005. https://doi.org/10.1016/j.ssi.2005.06.033

[44] P. A. Manning, J. D. Sirman, J.A. Kilner, "Oxygen self-diffusion and surface exchange studies of oxide electrolytes having the fluorite structure", Solid State Ionics, 93 [1–2], pp. 125–132, 1996. https://doi.org/10.1016/S0167-2738(96)00514-0

[45] C. Argirusis, G. Antonaropoulos, G. Sourkouni, F. Jomard, "Oxygen tracer diffusion in single crystalline yttrium silicate", Solid State Ionics, 262, 548–550, 2014. https://doi.org/10.1016/j.ssi.2014.01.026

[46] O. Yamaguchi, K. Takeoka, A. Hayashida, "Formation of alkoxy-derived $Y_3Al_5O_{12}$", J. Mater. Sci. Lett., 10, pp. 101–103, 1990. https://doi-org.inc.bib.cnrs.fr/10.1007/BF00721921

[47] E. Delon, F. Ansart, S. Duluard, J.P. Bonino, A.Malié, A. Joulia, P. Gomez, "Synthesis of yttria by aqueous sol-gel route to develop anti-CMAS coatings for the protection of EBPVD thermal barriers", Ceram. Int., 42 [12], pp. 13704–13714, 2016. https://doi.org/10.1016/j.ceramint.2016.05.169

[48] J. Fenech, C. Viazzi, J. P. Bonino, F. Ansart, A. Barnabé, "Morphology and structure of YSZ powders: Comparison between xerogel and aerogel", Ceram. Int., 35 [8], pp. 3427–3433, 2009. https://doi.org/10.1016/j.ceramint.2009.06.014

[49] D. Boyer, B. Derby, "Yttrium Silicate Powders Produced by the Sol – Gel Method , Structural and Thermal Characterization", J. Am. Chem. Soc., 86 [9], pp. 1595–1597, 2003. https://doi-org.inc.bib.cnrs.fr/10.1111/j.1151-2916.2003.tb03520.x

[50] R. Chrysafi, T. Perraki, G. Kakali, "Sol-gel preparation of $2CaO.SiO_2$", J. Eur. Ceram. Soc., 27 [2–3], pp. 1707–1710, 2007. https://doi.org/10.1016/j.jeurceramsoc.2006.05.004

[51] S. Kitaoka, T. Matsudaira, M. Wada, T.Saito, M.Tanaka, Y.Kagawa, “Control of Oxygen Permeability in Alumina under Oxygen Potential Gradients at High Temperature by Dopant Configurations”, J. Am. Chem. Soc., 97 [7], pp. 2314–2322, 2014. https://doi.org/10.1111/jace.12935

[52] E.J.L Schouler, N. Mesbahi,G. Vitter, “In situ study of the sintering process of yttria stabilized zirconia by impedance spectroscopy”, Solid State Ionics, 9-10, pp989-996, 1983. https://doi.org/10.1016/0167-2738(83)90120-0

[53] B. Boukamp, “Electrochemical impedance spectroscopy in solid state ionics: recent advances”, Solid State Ionics, 169(1-4), 65-73, 2004. https://doi.org/10.1016/j.ssi.2003.07.002

[54] B. Philippeau, F. Mauvy, C. Mazataud, S. Fourcade, JC. Grenier, “Comparative study of electrochemical properties of mixed conducting $Ln_2NiO_{4+\delta}$ (Ln=La, Pr and Nd) and $La_{0.6}Sr_{0.4}Fe_{0.8}Co_{0.2}O_3$“, Solid State Ionics 249–250, pp 17–25, 2013. https://doi.org/10.1016/j.ssi.2013.06.009

[55] A. Cordier, H.E. Khal, E. Siebert, M.C. Steil, “On the role of the pore morphology on the electrical conductivity of porous yttria-stabilized zirconia”, Journal of the European Ceramic Society, 39(7), pp 2518-2525, 2019. https://doi.org/10.1016/j.jeurceramsoc.2019.02.027

[56] A. Hashimoto, “The effect of H_2O gas on volatilities of planet-forming major: I. Experimental determination of thermodynamic properties of Ca-, Al-, and Si-hydroxide gas molecules and its application to the solar nebula”, Geochim Cosmochim Acta, 56, pp. 511–32, 1992. https://doi.org/10.1016/0016-7037(92)90148-C

[57] E.J. Opila, D.L. Myers, “Alumina volatility in water vapor at elevated temperatures”, J. Am. Ceram. Soc., 87, pp. 1701–5, 2004. https://doi-org.inc.bib.cnrs.fr/10.1111/j.1551-2916.2004.01701.x

[58] M. V. F. Schlupp, B. Scherrer, H. Ma, J. G. Grolig, J. Martynczuk, M. Prestat, and L. J. Gauckler,

"Influence of microstructure on the cross-plane oxygen ion conductivity of yttria stabilized zirconia thin films. Nonmetallic Inorganic Materials", Phys. Status Solidi, A209 [8], 1414–1422, 2012. https://doi-org.inc.bib.cnrs.fr/10.1002/pssa.201228248

[59] P. Yan, A. Mineshige, T. Mori, Y. Wu, G. J. Auchterlonie,J. Zou and J. Drennan, "Microanalysis of a Grain Boundary's Blocking Effect in Lanthanum Silicate Electrolyte for Intermediate-Temperature Solid Oxide Fuel Cells", ACS Appl. Mater. Interfaces, 5 [11], pp. 5307-5313, 2013. https://doi-org.inc.bib.cnrs.fr/10.1021/am401195e

[60] B. E. Deal, A. S. Grove, "General relationship for the thermal oxidation of silicon", J. Appl. Phys., 36 [12], pp. 3770–3778, 1965. https://doi.org/10.1063/1.1713945

[61] E. J.Opila, R. E. Hann, Paralinear Oxidation of CVD SiC in Water Vapor, J. Am. Ceram. Soc., 80 [1], pp 197-205, 1197. https://doi.org/10.1111/j.1151-2916.1997.tb02810.x

[62] J. M. Porras-Vázquez, E. R. Losilla, L. León-Reina, D. Marrero-López, M. A. G. Aranda, "Microstructure and oxide ion conductivity in a dense $La_{9.33}(SiO_4)_6O_2$ Oxy-Apatite", J. Am. Ceram. Soc., 92 [5], pp. 1062–1068, 2009. https://doi-org.inc.bib.cnrs.fr/10.1111/j.1551-2916.2009.03032.x

[63] B. Wang, Z. Lin, "A Schottky barrier based model for the grain size effect on oxygen ion conductivity of acceptor-doped ZrO_2 and CeO_2", Int. J. Hydrogen Energy, 39 [26], pp. 14334–14341, 2014. https://doi.org/10.1016/j.ijhydene.2014.03.142

[64] R. F. Klie, Y. Ito, S. Stemmer, and N. D. Browning, "Observation of oxygen vacancy ordering and segregation in Perovskite oxides", Ultramicroscopy, 86 [3–4], pp. 289–302, 2001. https://doi.org/10.1016/S0304-3991(00)00120-0

[65] W. J. Bowman, J. Zhu, R. Sharma, and P. A. Crozier, "Electrical conductivity and grain boundary

composition of Gd-doped and Gd/Pr co-doped ceria", Solid State Ionics, 272, pp. 9–17, 2015. https://doi.org/10.1016/j.ssi.2014.12.006

[66] R. M. Sullivan, "Reformulation of oxide growth equations for oxidation of silicon bond coat in environmental barrier coating systems ", J. Eur. Ceram. Soc., 39, pp. 5403–5409, 2019. https://doi.org/10.1016/j.jeurceramsoc.2019.06.057

[67] R. M. Sullivan, "On the oxidation of the silicon bond coat in environmental barrier coatings", J. Eur. Ceram. Soc., 41, pp. 557–562, 2021. https://doi.org/10.1016/j.jeurceramsoc.2020.07.019

[68] S. Arnal, "Relation microstructure/propriétés des barrières environnementales à base de silicate", PhD Thesis, University of Bordeaux, 2017. http://www.theses.fr/226192792

[69] M. Fernandez, "Modélisation de la durée de vie d'une barrière environnementale ", PhD Thesis, University of Bordeaux, 2019, http://www.theses.fr/2019BORD0270

[70] J.C. Fisher, "Calculation of Diffusion Penetration Curves for Surface and Grain Boundary Diffusion", J. Appl. Phys., 22, pp. 74-77, 1951. https://doi.org/10.1063/1.1699825

[71] T. Matsudaira, M. Wada, N. Kawashima, M. Takeuchi, D. Yokoe, T. Kato, M. Takata, S. Kitaoka, "Mass transfer in polycrystalline ytterbium monosilicate under oxygen potential gradients at high temperatures", J. Eur. Ceram. Soc., 41, pp. 3150–3160, 2021. https://doi.org/10.1016/j.jeurceramsoc.2020.07.045

[72] M. Wada, T. Matsudaira, N. Kawashima, M. Takeuchi, D. Yokoe, T. Ogawa, T. Kato, M. Takata, S. Kitaoka, "Effect of Water Vapor on Mass Transfer in Polycrystalline $Yb_2Si_2O_7$ under Oxygen Potential Gradients at High Temperatures", Acta Materialia, 201, pp. 373–385, 2020. https://doi.org/10.1016/j.actamat.2020.10.002

[73] J. D. Cawley and R. S. Boyce, “Solution to the diffusion equation for the double oxidation in dry oxygen including lazy exchange between network and interstitial oxygen“, Philos. Mag. B., 58 [4], 589-601, 1988. https://doi-org.inc.bib.cnrs.fr/10.1080/01418618808209939

[74] B.T. Richards, K.A. Young, Foucault de Franqueville, S. Sehr, M.R. Begley , H.N.G. Wadley, “Response of ytterbium disilicate-silicon environmental barrier coatings to thermal cycling in water vapor”, Acta Materialia, 106, pp. 1-14, 2016. https://DOI.org/10.1016/j.actamat.2015.12.053